

Review

Geogas-Carried Metal Prospecting for Concealed Ore Deposits: A Review of Case Studies in China

Qiang Wang^{1,2} , Xueqiu Wang^{3,*}, Zhizhong Cheng¹, Bimin Zhang³, Zezhong Du¹, Taotao Yan⁴, Huixiang Yuan¹, Xiaolei Li¹, Yu Qiao⁵ and Hanliang Liu^{3,*}

¹ Development and Research Center, China Geological Survey, Beijing 100037, China; wqgeochemistry@163.com (Q.W.); chengzhizhong69@163.com (Z.C.); dzezong@mail.cgs.gov.cn (Z.D.); yhx0593@163.com (H.Y.); lxiaolei@mail.cgs.gov.cn (X.L.)

² State Key Laboratory of Geological Processes and Mineral Resources, China University of Geosciences, Beijing 100083, China

³ Key Laboratory of Geochemical Exploration, Institute of Geophysical and Geochemical Exploration, Chinese Academy of Geological Sciences (CAGS), Langfang 065000, China; zbimin@hotmail.com

⁴ National Research Center for Geo-Analysis (NRCGA), Beijing 100037, China; yantaotao@mail.cgs.gov.cn

⁵ Zijin Mining Group Co., Ltd., Longyan 364200, China; qiaoyucugb@163.com

* Correspondence: wxueqiu@mail.cgs.gov.cn (X.W.); liuhanliang912@163.com (H.L.)

Abstract: Geogas-carried metal prospecting, an integral part of deep-penetrating geochemistry, is potentially effective in the geochemical exploration of concealed ore deposits. However, its principles and applicability remain controversial. This study summarizes and discusses the progress in geogas-carried metal prospecting in China. The method comprises three constituents: geogas, nanoparticles, and their vertical transportation. Researchers have failed to determine the exact contributions of different sources of geogas. Studies on Pb isotopes, rare earth element patterns of geogas, the comparisons between metals in soil, geogas, and ore geochemistry, and characteristics of nanoscale metals in earthgas (NAMEG), confirmed the relationship between NAMEG and concealed ore deposits. A statistical analysis of field experiments and applications showed that geogas-carried metal prospecting is applicable for the geochemical exploration of magmatic and hydrothermal Cu, Au, Zn, Pb, U, Sn, and Ag deposits and is suitable for most geochemical landscapes except deserts and cold swamps. Finally, genetic models of NAMEG anomalies were constructed. High-permeability migration channels are critical in the formation of NAMEG anomalies over concealed ore deposits. Future work entails applying geogas-carried metal prospecting to certain types of ore deposits and geochemical landscapes and studying NAMEG to provide quantitative information for targeting concealed ore deposits.

Keywords: deep-penetrating geochemistry; geogas-carried metal prospecting; concealed ore deposits; NAMEG; genetic model



Citation: Wang, Q.; Wang, X.; Cheng, Z.; Zhang, B.; Du, Z.; Yan, T.; Yuan, H.; Li, X.; Qiao, Y.; Liu, H.

Geogas-Carried Metal Prospecting for Concealed Ore Deposits: A Review of Case Studies in China. *Minerals* **2023**, *13*, 1553. <https://doi.org/10.3390/min13121553>

Academic Editor: Paul Alexandre

Received: 14 November 2023

Revised: 10 December 2023

Accepted: 13 December 2023

Published: 16 December 2023



Copyright: © 2023 by the authors. Licensee MDPI, Basel, Switzerland. This article is an open access article distributed under the terms and conditions of the Creative Commons Attribution (CC BY) license (<https://creativecommons.org/licenses/by/4.0/>).

1. Introduction

As the focus of geochemical exploration shifts from shallow to deep crustal levels, traditional geochemical methods are inadequate for the geochemical exploration of concealed ore deposits with various covers. Exploration geochemists proposed deep-penetrating geochemistry to solve the issue [1–5]. It identifies and strengthens weak geochemical anomalies derived from deep concealed ore deposits. Geogas-carried metal prospecting is an integral part of deep-penetrating geochemistry. The concept of geogas prospecting was initially proposed by Kristiansson and Malmqvist [6] and is based on the fact that the Rn anomaly over a deep concealed uranium ore deposit cannot be explained by ordinary diffusion. The principle of geogas prospecting suggests that Rn atoms are transported not only by ordinary diffusion but, more importantly, by ascending gas flow, which slowly carries them upward through the caprock towards the surface. Subsequently, geogas prospecting was

formally proposed as a novel and effective tool in the search for concealed ore deposits [7]. Geogas prospecting has been recognized under different names, including the molecular form of elements [8], particulate transport in the Earth [9], nanoscale metals in earthgas (NAMEG) [10], and the metal-in-soil-gas (MSG) technique [11,12]. In this study, geogas prospecting is referred to as geogas-carried metal prospecting to highlight its significance and uniqueness.

Geogas-carried metal prospecting has undergone nearly 40 years of development, and its principles and methods have been continuously improved. Chinese researchers have made significant progress in the fields of fundamental principles, the research and development of technical devices, experimental simulations, and field applications. In the 1990s, six topics for future research on geogas-carried metal prospecting were proposed as follows: (1) the composition, flow rate, and distribution pattern of geogas, and its relationship with the heterogeneity of the crust and mantle; (2) seasonal changes in geogas; (3) the applicability of geogas-carried metal prospecting in different climatic, geographical and geological conditions; (4) the migration of nanoscale-to-submicron-scale particles carried by geogas and the transformation of the particles into various active states in supergene environments; (5) locating concealed ore deposits with tactical geogas-carried metal prospecting; and (6) an analysis method for geogas [13]. Items (1), (2), and (4) are part of the study of the microscopic mechanism of geogas-carried metal prospecting, and items (3), (5), and (6) aid in the application of geogas-carried metal prospecting. This paper mainly focuses on items (3) to (5). Based on the summary of advances in the principles of geogas-carried metal prospecting, field experimentations, and applications, this study discusses the applicability of geogas-carried metal prospecting in different climatic, geographical, and geological conditions, and constructs typical genetic models and application scenarios of geogas-carried metal prospecting.

2. Advances in the Concept and Principle of Geogas-Carried Metal Prospecting

2.1. Evolution of the Concept of Gas-Carried Metal Prospecting

Geogas-carried metal prospecting originated from Rn anomaly research. Radon concentration in soil gas near the surface is an indicator of concealed uranium mineralization at depths equal to or more than 100 m. The half-life of Rn is 3.8 d, which suggests that a more powerful and faster transport mechanism to lift Rn to the surface must be in place instead of traditional diffusion [14]. Subsequently, the presence of microflows of geogas was demonstrated in 26 boreholes at three different sites, and the flow rates varied from 60×10^{-4} to $4 \text{ cm}^3/\text{min}\cdot\text{m}^2$ in a horizontally projected borehole area [15]. The trace elements in the geogas were further studied, and the results suggested that the elements carried by a stream of gas bubbles may be a potential prospecting method for concealed mineralization [16]. Based on these studies, the hypothesis of geogas-carried metal prospecting has been proposed: ore-related and pathfinder elements in concealed ore bodies were carried to the surface, forming geochemical anomalies, through the ascending microflow of gas bubbles. The geochemical anomalies are good indicators of geochemical exploration for concealed deposits. Several case studies primarily verified the effectiveness of geogas-carried metal prospecting. The studies included Au and As anomalies in snow immediately over a massive sulfide ore, Ni anomalies over a Cu–Ni mineralization covered by 1–2 m thick glacial till, Cu and Zn anomalies over the Golden Cross gold deposit covered by approximately 100 m of andesite, and Ni anomalies over massive sulfide ore bodies at a depth of approximately 1000 m [7]. Deep-penetrating geochemistry was proposed to explain geochemical anomalies in surface media over concealed ore deposits at a depth of several hundred meters [2–5,10,17,18]. Wang et al. [17] proposed the concept of ultrafine gold and concluded that a considerable amount of Au exists in the form of ultrafine particles in various media (e.g., rocks, stream sediments, and soils). Wang et al. [10] proposed the NAMEG method for the exploration of deep concealed ore bodies in overburden terrains, namely ultra-fine or nanoscale ore-related and pathfinder elements are carried by ascending gas flow from deep earth to the surface, forming geochemical anomalies over the concealed

ore deposits. Many researchers have directly discovered nanoscale metals in geogas, which strongly supports the NAMEG hypothesis [18–23].

The unanimous view is that geogas is naturally widespread [24], and sources of geogas include magma degassing [25–27], volcanic degassing [28], metamorphic degassing [29], thermal cracking of organic matter [30–32], microbial metabolism [33], supergene weathering [34–36], and barometric pumping of atmospheric gases [37,38].

The sampling medium of geogas-carried metal prospecting shows a strong relation between the compositions of geogas and the atmosphere. However, systematic studies on the composition of geogas, particularly trace gases, over various concealed ore deposits are instructive. Malmqvist and Kristiansson [14] verified the presence of microflows of ascending gas, which comprised N_2 , O_2 , Ar, and CH_4 , indicating a partly atmospheric source and secondary source. Both deep-earth degassing and gases derived from ore deposits are potential contributors to geogas. Scientists share a unanimous view on the process and occurrence of deep-earth degassing, although it is not discussed in this study. The basis of gas geochemical surveys of concealed ore deposits is the presence of ore-related gas geochemical anomalies, such as CO_2 , Hg, Ar, H_2S , SO_2 , and CH_4 , over concealed ore deposits, and other gas geochemical anomalies over concealed sulfide mineralizations [36,39–43], Rn and He anomalies over concealed uranium deposits [44,45], and hydrocarbon gas and He anomalies over oil and gas deposits [46,47].

The influences of different sources of gases on geogas-carried metal prospecting require further clarification. There are three possible scenarios: (1) both a gas geochemical survey and geogas-carried metal prospecting are sufficient to locate concealed ore deposits, if the gases released by concealed ore deposits are dominant in geogas; (2) only concealed ore deposits within the domain of supergene processes can be detected by geogas-carried metal prospecting, if deep-earth degassing and gases released by concealed ore deposits are negligible; or (3) gases originating from intense deep-earth degassing rather than ore deposits flow through concealed ore bodies and transport some ore-related metals to the surface.

2.2. Compositions and Morphology of Nanoscale Metals in Earthgas (NAMEG)

NAMEG are a hotspot of current research. Detailed studies have been conducted on the characteristics of NAMEG, including size, shape, component, structure, and genesis of polymerization (Table 1). Generally, the features of nanoparticles are as follows: (1) most individual nanoparticles are pellet-shaped, irregular polygons, oval-shaped, or nearly spherical, ranging in size from a few nanometers to hundreds of nanometers; (2) several individual nanoparticles can aggregate into cluster-like aggregates, and particle aggregates are elliptical, globular, catenarian, or irregular in shape, ranging in size from tens of nanometers to hundreds of nanometers; (3) some nanoparticles have a crystal exterior and an ordered crystal structure; and (4) individual nanoparticles consist of a single component or are multi-component alloys. Remarkably, the composition of most nanoparticles is very complex, including ore-forming elements, associated elements, and other elements (e.g., Si, O).

Table 1. Characteristics of ore-related NAMEG over ore deposits in China (n = one to nine).

Deposit	Composition	Size (nm)	Morphology	Reference
Dongji Au deposit, Shandong	Si, Al, S, Ca, Fe, Mg, K, Cu	$n-n \times 10^2$	Amorphous and microcrystalline aggregates	[18]
Changkeng Au deposit, Guangdong	Au, Hg-S-O-Si-Cl-K, Pb-N-O-Sn, Pb-S-O-Fe, Zn-Sn-O-Si-Br-Fe	$n \times 10-n \times 10^2$	Irregular, needle-shaped, or rhombic plate-shaped	[48]
Tongchanghe Cu mine, Guizhou	Cu, Cu-Fe, Cr-Fe-Cu	Individuals: 5–40; aggregations: 20–150	Individuals: subcircular, elliptical, polygonal, or elongate; aggregations: subcircular or elliptical	[49]

Table 1. Cont.

Deposit	Composition	Size (nm)	Morphology	Reference
Fankou Pb-Zn deposit, Guangdong	Pb-(Mo/Cu), Zn-Sn-Cr, Zn-S-O, Pb-Zn-(Mo), Pb-Zn-Sb-As-Ge	10–300	Single particles: irregular, spherical, or trigonal plate-shaped; aggregations: globular, catenarian, or irregularly shaped	[50]
Zhou'an Cu-Ni deposit, Henna	Cu, Cu-Fe, Cu-Ti, Cu-Ag, Cu-Cr, Cu-Fe-Mn	n–n × 10 ²	Spherical, ellipsoid, grape-shaped, or polyhedral spheres; with a crystal appearance and an ordered crystal structure	[21]
Kaxiutata Fe deposit, Inner Mongolia	F-, Cu, Zn, Bi, M-, Pb	n × 10–n × 10 ²	Semi-oval, triangular, cloud-like, horsetail, elliptical, or irregular	[51]
Dongshengmiao polymetallic pyrite deposit, Inner Mongolia	S-(Cu/Zn/Pb/Mo), S-Fe-Zn-(Pb), S-Fe-Cu-(Mo), Cr-Mn-Fe	5–400	Sub-circular, elliptical, or irregular	[52]
	C-(Fe/Zn/Au/Cu/Pb)	n × 10–n × 10 ²	Sub-circular or ellipsoid	[53]
Jinwozi Au deposit, Xinjiang	Cu, Cu-Fe-Zn, Cu-Ti, Cu-Au	n × 10–n × 10 ²	Spherical, ellipsoid, grape-shaped, or polyhedral spheres; with a crystal appearance and an ordered crystal structure	[54]
Yueyang Ag-Au-Cu ore block, Fujian	Au, Cu, Au-Cu-Mo, Au-Cu, Cu-Co-Mo, Cu-Fe	n–n × 10 ²	Granular, spherical, polygonal spherical, or cluster-like aggregates; with a crystal appearance, and an ordered crystal structure	[22,54]
Kafang Cu deposit, Yunnan	Cu-Ag-Co-Fe, CuSO ₄ , WO ₃ , TiO ₂ , Pb and Fe oxides	20–300	Irregular, round, slab-flaky, or quadrilateral	[55]
Qingmingshan Cu-Ni sulfide deposit, Guangxi	Fe-Co-(Cu/Zn)	50–500	Nearly elliptical, nearly spherical, drop-shaped, or nearly rectangle	[56]
Bingba Cu deposit, Guizhou	Fe-Cu-Zn-(Mn/O/As), Zn-Fe-Kr-SiO ₂ , Pb-Kr-Zn-O	n–300	Chain-shaped, round, and irregular	[57]
Gongpoquan porphyry Cu deposit, Gansu	Pb, Cu, Pb-Zn, Cu-Fe-(Mn/Ti), Mn-Fe-Ti, Cu-Ti	n–n × 10	Sphere, or polygonal granule; with an ordered structure	[58]
Shenjiayao Au deposit, Henna	Cu, Cu-Au-(Pb), Cu-Ti-Fe-Mo, Cu-Au-Ag-Mg-Fe-S	n–n × 10 ²	Sphere, oval, polygon, single pellets, chain, or irregular pellets; with an ordered internal structure	[54,59]
Bairendaba Pb-Zn deposit, Inner Mongolia	Cu, Pb, Cu-Si-O, Zn-Fe-O, Zn-Y-Na-S-O, Pb-K-Na-S-O	n × 10–n × 10 ²	Round, elliptic, ball-shaped, or flocculent shape	[60]

Detailed studies on the redox state of NAMEG also have been conducted, and the results show the presence of nanoparticles with high oxidation valence in geogas over metal sulfide deposits. Examples include high-oxygen and low-sulfur nanoparticles in geogas over the Bairendaba lead–zinc deposit [60], Fe, Co, and S-oxide particles (hematite and SO₃) in geogas over the Qingmingshan Cu-Ni sulfide deposit [56], and iron and

copper oxide particles in geogas over the Daheishan basalt–copper deposit [61]. Although the assumption that these highly oxidized nanoparticles originate from the surrounding rocks cannot be entirely dismissed, we inferred that the NAMEG are closely related to supergenesis; that is, the NAMEG may be the product of weathering or were probably transformed by supergenesis.

Statistical results show that deposits with abundant metal-bearing nanoparticles primarily include Au, Cu (Ni), and Pb-Zn deposits. Generally, NAMEG over concealed ore bodies consist of native metals, alloys, compound metals with Si, Al, Ca, O, and P, oxides, and hydroxides. First, NAMEG over different types of deposits have different compositions. Cu-bearing nanoparticles are abundant in geogas over concealed Cu-Ni deposits, whereas Au-bearing nanoparticles are abundant in geogas over concealed Au deposits (Figures 1 and 2). Even within the same deposit type, the specific composition of NAMEG is also different. For example, the Zhou’an and Qingmingshan Cu-Ni sulfide deposits are basic–ultrabasic Cu-Ni deposits. The NAMEG in the Zhou’an sulfide deposit include native Cu, Cu-Fe, Cu-Fe-Mn, Cu-Ag, Cu-Cr, and Cu-Ni alloys, and compound metals with Si, Al, Ca, O, and P (Figure 1a–d) [22]. The NAMEG in the Qingmingshan sulfide deposit include Cu-Fe-Co, Zn-Fe-Co, and Fe-Co alloys, Fe-Co and Fe oxide (hydroxide), and other oxide particles (e.g., Si oxide, calcium carbonate, calcium hydroxide, and sulfur trioxide) (Figure 1e–l) [56].

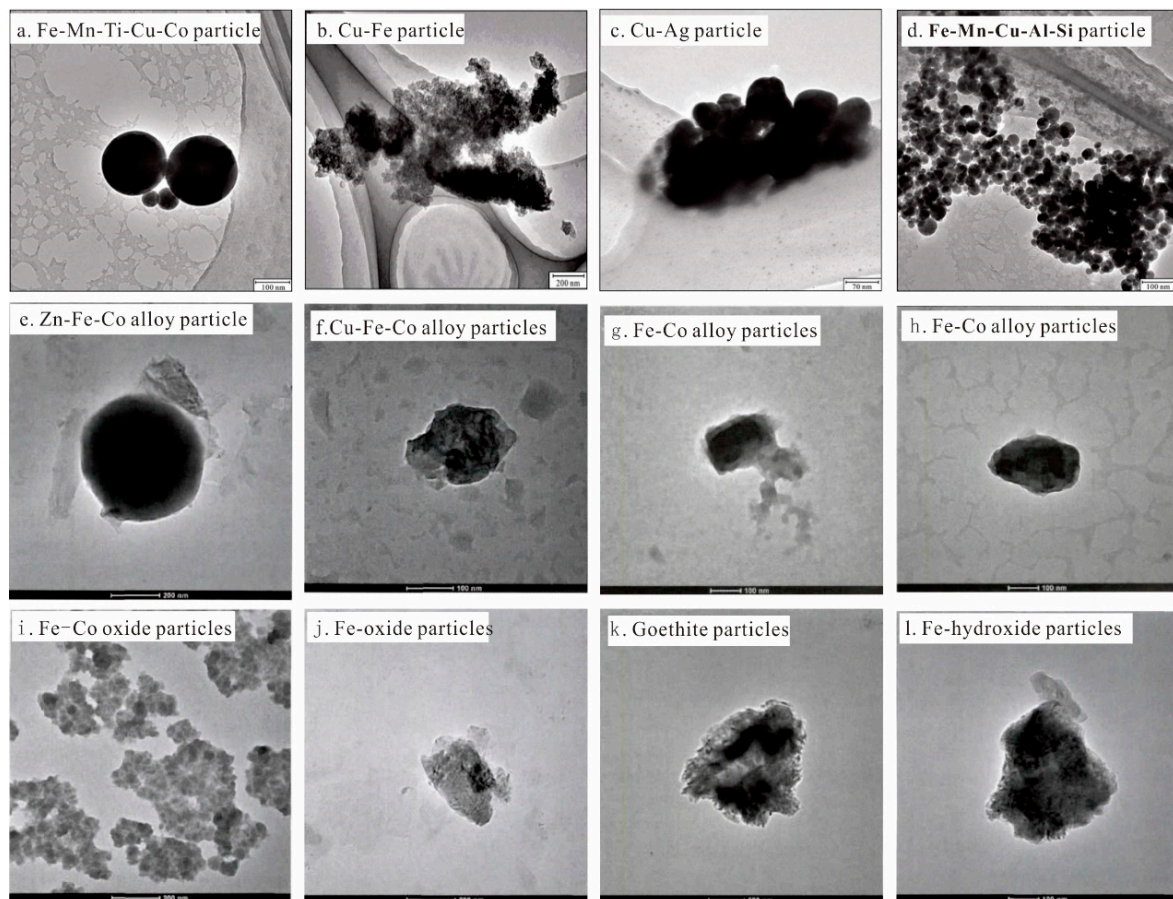


Figure 1. Nanoscale particles in geogas and soil over the Zhou’an (a–d) [22] and Qingmingshan (e–l) [56] Cu-Ni sulfide deposits. (a) Fe-Mn-Ti-Cu-Co nanoparticles in geogases; (b) Cu-Fe nanoparticles in geogases; (c) Cu-Ag nanoparticles in soils; (d) Fe-Mn-Cu-Al-Si nanoparticles in soils; (e) Zn-Fe-Co nanoparticles in geogases; (f) Cu-Fe-Co nanoparticles in geogases; (g) Fe-Co nanoparticles in geogases; (h) Fe-Co nanoparticles in geogases; (i) Fe and Co-oxide nanoparticles in geogases; (j) Fe-oxides nanoparticles in geogases; (k) goethite nanoparticles in geogases; and (l) Fe-hydroxide nanoparticles in geogases.

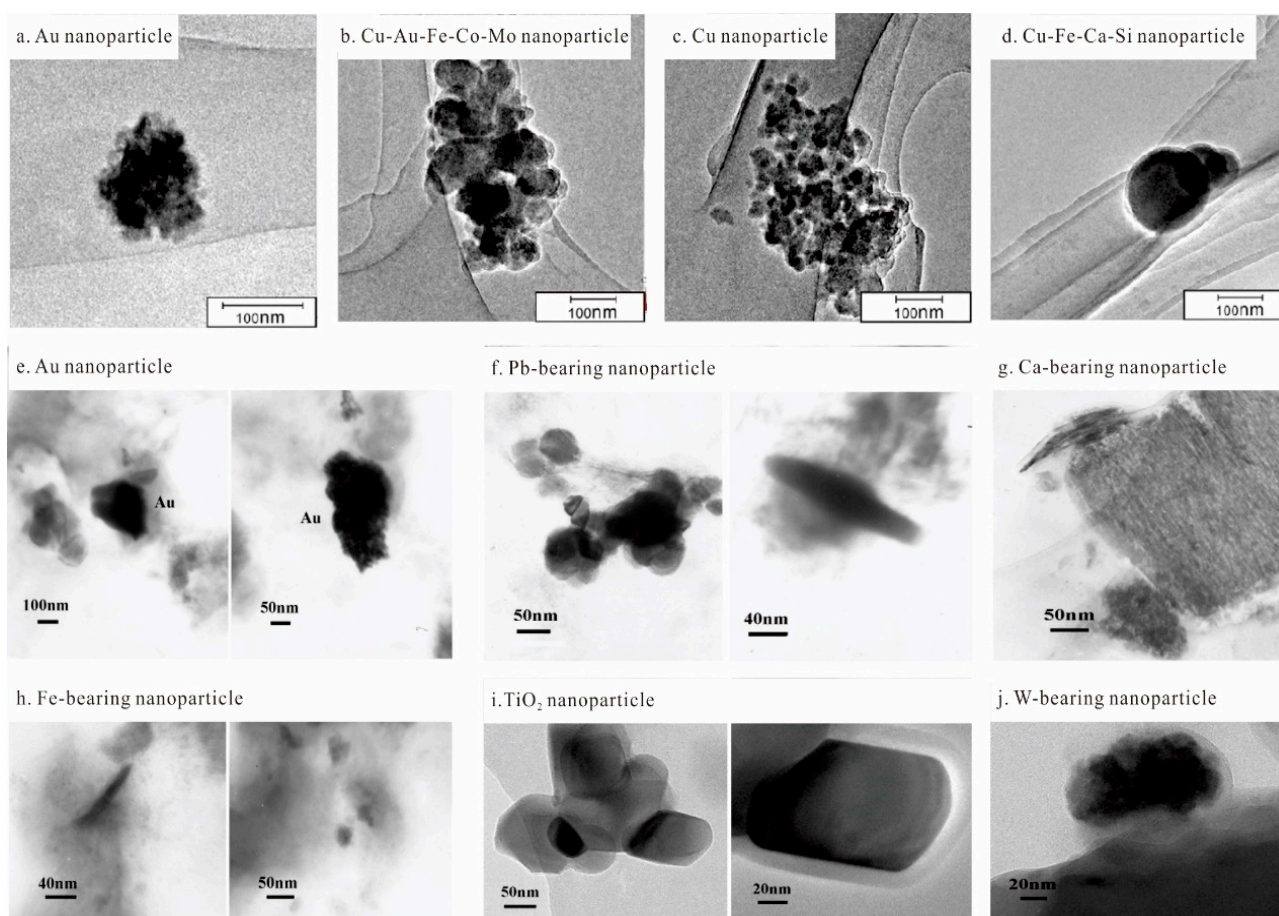


Figure 2. Nanoscale particles in geogas and soil over the Yueyang Ag-Au-Cu ore block (a–d) [23] and Changkeng Au deposit (e–j) [48]. (a) Au nanoparticles in geogas; (b) Cu-Au-Fe-Co-Mo nanoparticles in geogas; (c) Cu nanoparticle aggregate in soil; (d) Cu-Fe-Ca-Si nanoparticles in soil; (e) Au nanoparticles in geogas; (f) spherical and cudgel Pb-bearing nanoparticles in geogas; (g) Ca-bearing nanoparticle assemblage in geogas; (h) needle-shaped and irregular Fe-bearing nanoparticles in geogas; (i) TiO_2 nanoparticles in geogas; and (j) W-bearing nanoparticle assemblage in geogas.

2.3. Sources of Nanoscale Metals in Earthgas (NAMEG)

Metal-bearing nanoparticles are widespread in nature (e.g., ore deposits, surrounding rocks, fault gouges, regolith, and geogas) [22,62–71]. NAMEG can be divided into two categories. The first is NAMEG that are irrelevant to mineralization and appear in both anomalous and background areas. These nanoparticles, mainly consisting of Si, Ti, O, and C, have little significance for geochemical exploration. The second is NAMEG that are closely related to mineralization and provide useful information for targeting deep concealed ore deposits; these ore-related nanoparticles occur in higher concentrations in geogas over concealed ore deposits than in background areas, although the total concentrations of NAMEG over concealed ore deposits remain low.

Another significant challenge in geogas exploration is determining that NAMEG are derived from concealed ore deposits rather than the weathering of surrounding rocks or nearby ore outcrops. At present, the evidence that NAMEG originate from concealed ore deposits is primarily derived from isotopes, rare earth element (REE) patterns, statistical and comparative analyses of geogas components from background areas and anomalous areas, and the geochemical components of concealed ore deposits. Among them, statistical and comparative analyses of their compositions provide the best evidence; that is, there are more abundant ore-forming and associated elements in geogas over concealed ore deposits than in those from background areas. Many studies have investigated the origination of

NAMEG [11,16,17,22,72–75], which will be subsequently discussed. The following section primarily presents evidence of isotopes, REE patterns, and geochemical comparisons of geogas-carried metals and soils.

2.3.1. Composition Comparison

A summary of field experiments and applications of geogas-carried metal prospecting in China was conducted to demonstrate the applicability of geogas-carried metal prospecting (Table 2). The key items include element association, buried depth of the concealed ore body, sampling method, hole depth, and trapping medium.

Table 2. A summary of field experimentations and applications of the NAMEG method in China.

Deposit or Area	Element Association	Buried Depth (m)	Sampling Method	Hole (or Sampling) Depth (m)	Trapping Medium	References
Liaojie Au ore deposit, Yunnan	Zn, As, Sb, Cs, Cr, La, Sm, Sc, K, Au, Ag	50~200	SS			[76]
Dongyi Au deposit, Shandong	Au, Cr, Zn, Sb, As, La, Sm, Na, Sc, Fe	~150; 200~400	SS	0.5~0.6		[72,77]
Dayinggezhuang Au deposit, Shandong	Au, As, Sb, Hg, Bi, K	250~330	SS	0.6	Aqua regia and foam	[16]
Chaihulanzhi Au deposit, Inner Mongolia	Au	75~100	AS	(0.5–0.7)	Foam plastic	[78]
Budunhua Cu deposit, Inner Mongolia	Cu, Au	430~530	AS	(0.5–0.7)	Foam plastic	[78]
Laoyanghao Au ore district, Inner Mongolia	Au, Ag, Cu, Pb, Ni	~100	AS	0.5~1.0	Foam plastic	[79]
Salbulack Au deposit, Xinjiang	Au, Sb, Zn, Fe, K, Sc		AS	0.4~0.5		[77]
Mofancun prospecting area, Sichuan	Au, Sb, As, K, Al, Fe, La, Zn		AS	0.4~0.5		[77]
Chaihuolanzi Au deposit, Inner Mongolia	Au					[80]
Tuanjie Au deposit, Heilongjiang	Au, As, Sb, La, Sm, Se		SS	0.4~0.5	Foam plastic	[81]
Gadaban district, Qinghai	Au, Ag, Cu, Zn, Ba, Sr		AS	(0.4)	Aqua regia, nitric acid, and foam plastic	[82]
Heihe Basin, Qinghai	Au, Ag, Cu, Pb, Zn		AS	0.4~0.8 (0.35)	Aqua regia and nitric acid	[83]
Beiqilian area (Pb-Zn ore body)	Au, Ba, Zn, Pb	150	AS	0.5~0.8	Aqua regia	[84]
Jiaolongzhang Pb-Zn deposit, Gansu	Cu, Pb, Zn, Cd, Ag, Bi, Ni, Sb, Tb, Tl, Yb	~100	AS	0.5–0.8; 0.6–1.0 (0.4–0.5)	Nitric acid	[73,85,86]
Lashuixia Cu–Ni deposit, Qinghai	Cu, Pb, Zn, Ag, Mn, Co		AS	0.5~0.8 (0.3~0.4)	Aqua regia	[87,88]

Table 2. Cont.

Deposit or Area	Element Association	Buried Depth (m)	Sampling Method	Hole (or Sampling) Depth (m)	Trapping Medium	References
Zhangquanzhuang Au Deposit, Hebei	Cu, Pb, Zn, Cd, Ag, Bi, Ni, Sb, Tb, Tl, Yb	~50	AS	-	-	[49,85,88,89]
Wangjiazhuang Cu ore deposit, Shandong	Ag, Cu, Pb, Zn, Bi, Co, Ni, Sb	80–120	AS	-	-	[85,89]
Changpai U exploration area, Guangdong	U	600, 700	AS		Nitric acid	[90]
Dachang Sn polymetallic ore deposit, Guangxi	Zu, Cu, Pb, W, Mo, Bi, Rb, Cd, Hg, Au	>800	AS	(0.8)	Nitric acid	[91]
210 Au deposit, Xinjiang	Au, Ag, Cu, Fe, Sb, Ca, REE	4.5~15	AS	(0.5–0.8)	Aqua regia and foam	[65,92]
Zn-Cu deposits in the Dachang area, Guangxi	Cu, Pb, Zn, W, Mo, Bi, Rb, Cd, Hg, Au	>800	AS	(0.8)	BV-III grade pure nitric acid and deionized water	[76,93]
Dongshan Pb-Zn deposit, Yunnan	Pb, Zn, Cu, Au, As, La, Sr		AS			[94]
Huangshaping-Liaojiawan Ag-Pb-Zn polymetallic ore deposit, Hunan	Cu, Pb, Zn, As, W, Mo, Bi, Mn, Ag	180	AS	0.5, 0.8	BV-III grade pure nitric acid and deionized water	[77,93,95]
Lijiaduan U deposit, Hubei	U, Pb, Mo, Bi, As, Cu, Mn, Ag, Cd, W, Th, Sc, Li, Cs, Sr, REE		AS			[96]
Renhua U exploration area, Guangdong	U, REE, Cd, Mn, Pb, Zn	110~190; >560	AS	(0.8)	BV-III grade pure nitric acid and deionized water	[74]
Dongshengmiao polymetallic pyrite deposit, Inner Mongolia	Fe, Cu, Pb, Zn	Tens to hundreds	SS		Plastic film	[52]
Yueyang Ag-Au deposit, Fujian	Ag, Au, Cu, As	80~700	-	-	Aqua regia and foam plastics	[75]
Shengjiayao Au deposit, Henan	Au, Cu, Pb, Zn, Ag	<350	AS	0.6–0.8	Aqua regia and foam	[54,59]
Hongshanzi U prospecting area	U, Pb, Cr, Nd, Th, Mo, Cu, Zn, Ag, W	150~350	AS	0.7–0.8	Aqua regia and foam plastic	[97]
Xitian area (W-Sn polymetallic ore deposit), Hunan	Sn, W, Pb, Zn, Ag, Cu, Ni, Co, Sb, Bi, Mo	190 (bottom elevation)	AS	0.5~0.8	Nitric acid	[98]
Tianyu Cu-Ni deposit, Xinjiang	Ni, Co, Cu, Fe, V		AS	0.5~1.0	Nitric acid	[99]

Table 2. Cont.

Deposit or Area	Element Association	Buried Depth (m)	Sampling Method	Hole (or Sampling) Depth (m)	Trapping Medium	References
Debao Cu deposit, Guangxi	Cu, Pb, Zn, Bi, Ni, Sb, Ag, Cd, Mn, Ce	100~300	AS	0.6~1.0 (0.4~0.5)	Nitric acid	[100]
Jiajika superlarge Li-polymetallic deposit, Sichuan	Li, Be, Rb, Cs, Na, B	~100	AS	0.5~0.6	Nitric acid	[101]

Notes: SS and AS represent static sampling and active sampling, respectively.

Different ore deposits are characterized by different element associations. These characteristic element associations suggest that ore-related nanoparticles carried by geogas can penetrate covers and form geochemical anomalies over concealed ore deposits, although they may be transformed and intervened by supergene processes.

The detection depth of geogas-carried metal prospecting requires further research. In the majority of the cases, the detection depth is less than 500 m. Cases where the depths of concealed ore deposits are >800 m are scarce (e.g., Dachang Sn polymetallic ore deposit [90] and Zn-Cu deposits in Dachang area [76,93]). The known maximum detection depth of geogas-carried metal prospecting is approximately 1000 m for a massive sulfide ore deposit [7].

In early field experiments and applications, static sampling was the primary sampling method, which is time-consuming. With the development of sampling devices, filter membranes, which can filter out larger-sized particles derived from soils, have been integrated into sampling devices; sampling using such devices is referred to as active sampling, which is efficient and time-saving. Currently, active sampling is the mainstream sampling method.

The trapping medium is critical for the successful application of geogas-carried metal prospecting. Common trapping media include aqua regia, nitric acid, and foam plastics. For adequate results, the contents of target elements in the trapping medium should be negligible, or sufficiently low enough to have minimal effects on the measurement results of geogas-carried metal prospecting [12]. Tailored trapping media are required for different deposits because the trapping capacities of various trapping media for different elements are distinct. Field experiments and applications suggest that the capture ability of aqua regia for Au, Ag, Cu, Zn, and other elements is better than that of nitric acid, and foam plastic has certain advantages for Au adsorption [10,12,16,82].

2.3.2. Morphology of Nanoscale Metals in Earthgas (NAMEG)

Abundant metal-bearing nanoparticles are present in geogas and their morphologies are characteristic and instructive. Here, Au was used to demonstrate the morphological characteristics of metal-bearing nanoparticles.

Various Au-bearing nanoparticles have been observed in ore rocks, arsenian pyrite, fault gouges, and other materials (Figure 3). Reich et al. [102] revealed that abundant Au nanoparticles were disseminated throughout an arsenian pyrite matrix, and individual Au nanoparticles showed a rounded shape and well-defined boundaries (Figure 3(b1,b2)). Zhang et al. [68] observed irregular Au-bearing particles and roughly circular Au-bearing particle aggregation in fault gouges in the Shenjiayao gold deposit (Figure 3(c1,c2)). These results verify the presence of abundant Au-bearing nanoparticles in rocks which may be a potential source of metals in geogas.

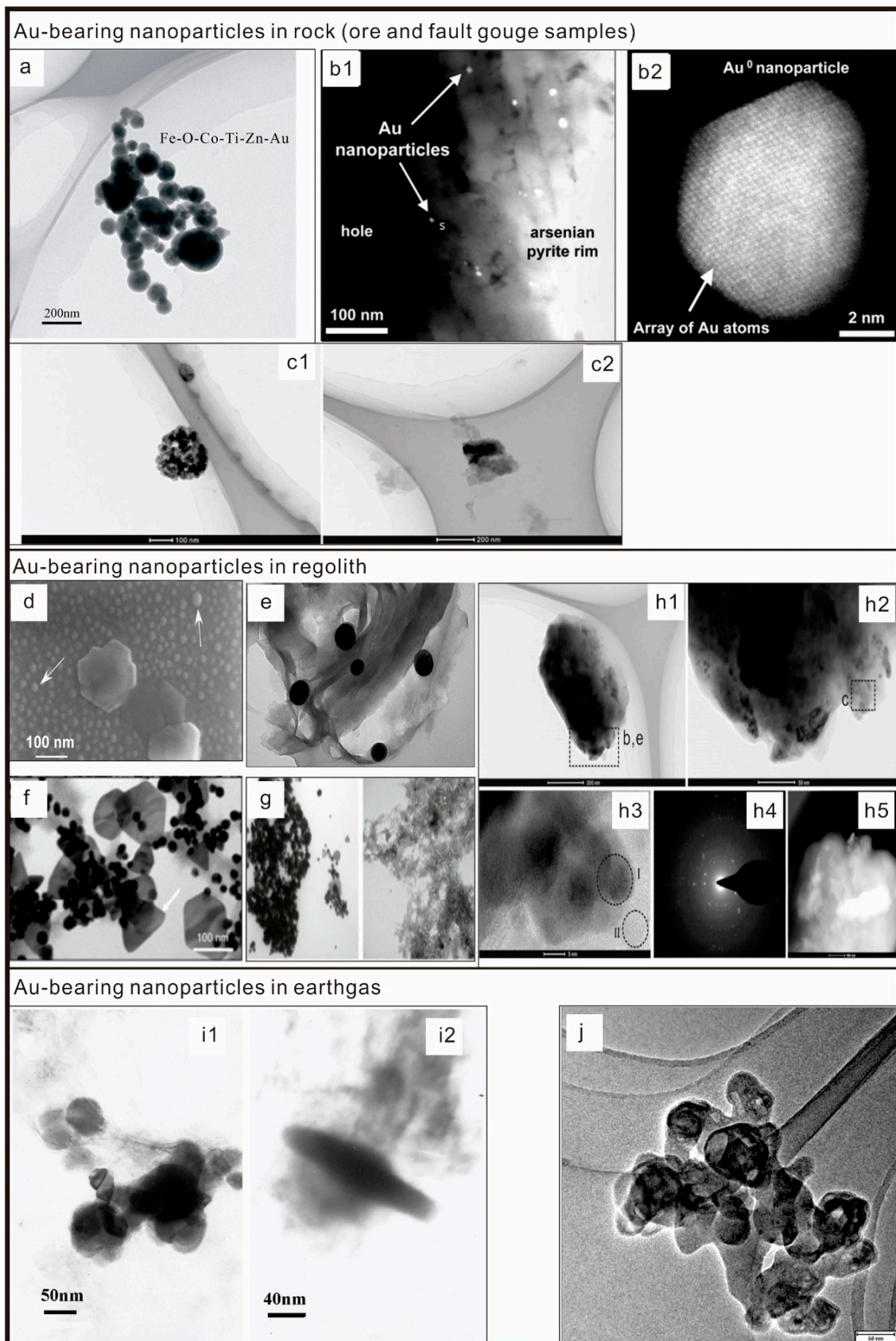


Figure 3. Various Au-bearing nanoparticles in rock, regolith, and geogas. (a) Au-bearing nanoparticles in an ore rock sample from the Shanggong gold deposit [69]; (b1,b2) Au-bearing nanoparticles in arsenian pyrite [102]; (c1,c2) Au-bearing nanoparticles in fault gouges from the Shenjiayao Gold

Deposit [68]; (d) 20 nm nanospheres arrowed in the background next to coarser Au nanoparticles hosted on larger gold particles in a weathered quartz fracture [64]; (e) colloidal gold nanoparticles in an ultrathin section of the sediment [103]; (f) Au nanoparticles produced from the exposure of delftibactin to Au(III)-chloride, the arrow shows the co-precipitation of quasi-spherical nanoparticles and octahedral platelets due to biomineralization [104]; (g) gold nanoparticle formation by microbial metallophores [105]; (h1–h5) Au-bearing nanoparticle in soil sample over the Shenjiayao Gold Deposit [68]; (i1,i2) Au-bearing nanoparticle in the geogas over the Changkeng concealed gold deposit [48]; and (j) Cu-Au bearing nanoparticles in geogas over the Shenjiayao gold deposit [59].

Au-bearing nanoparticles carried by geogas can be divided into two categories: those formed by supergene processes (e.g., weathering), and those directly derived from concealed ore bodies or primary halos. The morphologies of the former Au-bearing nanoparticles are generally distinct from those of the endogenous nanoparticles (e.g., ore body and alteration). Studies on supergene processes have shown that microbial metallophores can result in the formation of colloidal, quasi-spherical, octahedral, and bacterioform gold nanoparticles, which are abundant in the surface medium of Au grains (Figure 3d–g) [62,104,105]. A detailed study on gold grains suggested that concavities, accounting for 10%–40% of the total grain surface area, contain clay-sized minerals, microorganisms, and secondary Au nanoparticles, which are formed by microorganisms and occur as spheroidal colloids and octahedral platelets [103]. Au nanoparticles can additionally form microcrystals, sheet-like Au, branched Au networks and overgrowths, and secondary rims during the biogeochemical cycling of gold [106]. The Au-bearing nanoparticles derived from concealed ore bodies or primary halos are therefore distinct from supergene Au-bearing nanoparticles. As suggested by Zhang et al. [68], Au-bearing nanoparticles directly derived from concealed ore bodies or primary halos exhibit an irregular shape and crystalline nature (Figure 3 (h1–h5)).

The Au-bearing nanoparticles in geogas are irregularly shaped assemblages [48,59], which are different from the Au-bearing nanoparticles formed by biogeochemical and chemical processes in supergene environments, although some of the supergene Au-bearing nanoparticles have an irregular shape. This difference suggested that NAMEG are derived from concealed ore bodies and primary halos rather than from Au-bearing nanoparticles formed by supergene biogeochemical and chemical processes.

2.3.3. Lead Isotope Composition

Pb isotopes provide the most direct evidence for the correlation between geogas and concealed ore deposits, particularly Pb-rich metal sulfide deposits, which provide a solid foundation for the source analysis of NAMEG. Theoretically, the significant differences in Pb isotope compositions between background and anomalous areas, and the considerable similarities among Pb isotope compositions between anomalous areas and concealed ore deposits, indicate the contribution of concealed ores to the Pb isotope composition in geogas.

Previous studies have shown that Pb isotope compositions in geogas have genetic relationships with concealed ore deposits. Wang and Gao [73] and Wan et al. [89] conducted detailed studies on the Pb isotope compositions in geogas from the background and anomalous areas, loess, red layer, wall rocks, and ores in the Jiaolongzhang Pb-Zn deposit, Gansu, and revealed that the Pb isotope compositions in the geogas anomalies over the concealed orebodies are different from those in the background, falling between the Pb isotope compositions of wall rocks and ores (Figure 4a). The results support the contribution of concealed ore deposits to anomalous Pb in the geogas. Xu et al. [107] suggested that the Pb isotope compositions in geogas are similar to those in the ore samples of the Wangjiazhuang copper deposit in Zouping, Shandong Province, and the significant difference between the Pb isotope compositions in geogas from the anomalous areas and overlying soil demonstrates that soil Pb composition is not a dominant factor for the Pb

isotope compositions in geogas (Figure 4b). The aforementioned case studies strongly indicate the contribution of concealed ore deposits to NAMEG.

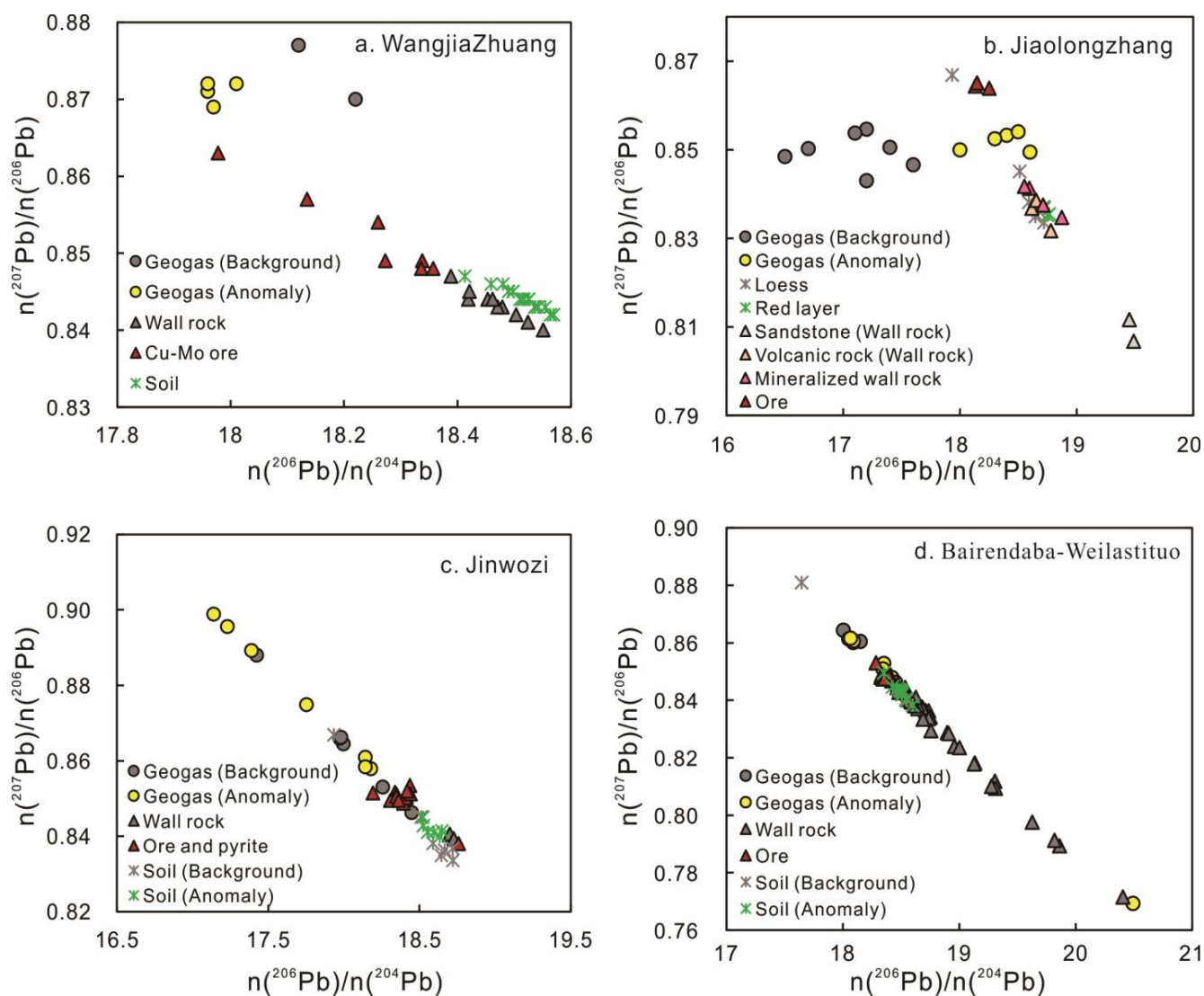


Figure 4. $^{207}\text{Pb}/^{206}\text{Pb}$ vs. $^{206}\text{Pb}/^{204}\text{Pb}$ plot in wall rocks, caprocks, geogas, and ores in the Wangjiazhuang copper deposit (a), the Jiaolongzhang Pb-Zn deposit (b), the Jinwozi Au deposit (c), and the Bairendaba-Weilastituo Polymetallic deposit (d) (Pb contents in ores, wall rocks, and soil refer to their mass fractions, and Pb contents in gases refer to their mass concentrations) [73,89,107,108].

However, the Pb isotope compositions in the geogas (background and anomalous areas), soil, ore, and wall rock in the Jinwozi Au deposit, Xinjiang, and the Bairendaba-Weilastituo polymetallic ore deposit in Inner Mongolia failed to verify the genetic relationship between the Pb isotope composition in geogas from anomalous areas and concealed ore deposits. In the Jinwozi Au deposit, the Pb isotope compositions in the geogas from the background and anomalous areas were not significantly different, which may be caused by the limited difference in Pb isotope compositions between the ore and wall rock (Figure 4c). In contrast, Pb isotope compositions in the geogas from the background and anomalous areas in the Bairendaba-Weilastituo polymetallic ore deposit also showed no significant difference, although the difference between the Pb isotope compositions from the ore and wall rock was relatively significant (Figure 4d) [108].

The minor difference in Pb isotope compositions between geogas from the background and anomalous areas and the weak genetic relationship between Pb isotope compositions

in geogas from anomalous areas and concealed ore deposits may be a result of two factors. First, Pb isotope composition in geogas may be influenced by the Pb isotope compositions of the rocks through which the gas flows upward. Therefore, the Pb isotope compositions in geogas from anomalous areas are significantly different from those of deep concealed ore deposits, because thick caprock dominates Pb isotopic compositions in geogas. Second, the Pb isotopic composition of the trapping solution may be another factor that affects the traceability of Pb isotopes (Figure 5) [108].

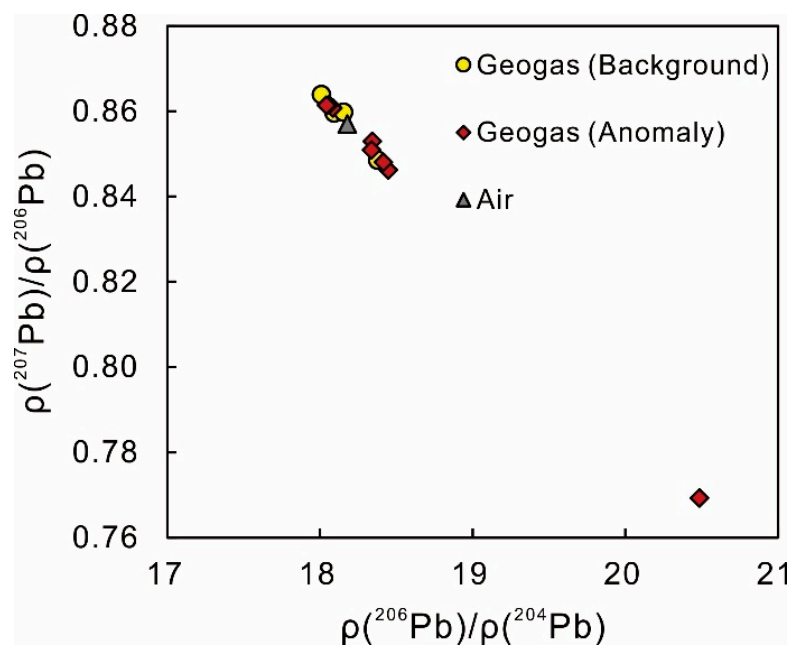


Figure 5. Pb isotopic characteristics of geogas and air samples in the Bairendaba-Weilasituo poly-metallic sulfide ore deposit, Inner Mongolia [108].

2.3.4. Rare Earth Element Pattern

Comparative studies have been conducted on the rare earth distribution patterns of ores, surrounding rocks, soils, and geogas over concealed ore deposits and in background areas of different mining sites, to determine the correlations between geogas anomalies and concealed ore deposits. The comparative study conducted on the Zhangquanzhuang gold deposit by Gao et al. [109] revealed that the REE patterns of geogas were similar to those of the ores, and that the total REE in the geogas over concealed ore deposits was higher than that of the background geogas samples. Zhou et al. [93] suggested that the REE patterns in the geogas over concealed ore deposits have a distinct inheritance relationship with the metamorphic–metasomatic granite and skarn in the Huangshaping Pb–Zn deposit, Hunan. Wang et al. [110] revealed that the REE patterns of geogas and ore samples in the Jinwozi 210 gold deposit in Xinjiang are similar, characterized by the relative enrichment of light rare earths, the relative loss of heavy rare earths, and no significant Eu and Ce anomalies. However, this study still requires further research on the REE patterns of the surrounding rocks and soils to support the correlation between geogas and concealed ore deposits. Wan et al. [86] conducted a comprehensive study on the REE patterns of background soils and geogas, as well as ores, wall rocks, and geogas in anomalous areas in the Jiaolongzhang Pb–Zn deposit. The results suggested that the geogas REE from the anomalous area is characterized by higher total REE, and small fluctuations in REE contents, which may also be caused by the REE characteristics of the wall rocks and regolith and the analytical detection limit [86,109]. However, effectively determining whether the REE in the geogas from the anomalous area originates from concealed ore deposits is challenging because ores and wall rocks have similar REE patterns.

2.3.5. Relationship between Soil and Ore-Related Nanoscale Metals in Earthgas (NAMEG)

Excluding soil as a major contributor to NAMEG is crucial. If the NAMEG primarily originate from soil, the significance of geogas-carried metal prospecting will no longer exist because geogas-carried metal prospecting cannot provide information on concealed ore deposits in areas with exotic cover.

Pb isotope studies of the Jinwozi Au deposit, Wangjiazhuang Cu deposit, and Bairendaba-Weilasituo polymetallic sulfide ore deposit have revealed that the Pb isotopic compositions of the geogases and soils in anomalous areas are different. Considering that Pb isotopic compositions may also be affected by other factors, additional evidence is required to conclude that the NAMEG primarily originate from concealed ore deposits.

Field studies have shown that there are three distinctive relationships among concealed ore deposits, soil, and geogas in geochemical exploration: the coexistence of geogas and soil geochemical anomalies over concealed ore deposits, the presence of geogas anomalies without soil anomalies over concealed ore deposits, and presence of soil anomalies without geogas anomalies in transported areas.

In the first scenario, both geogas and soils over concealed ore deposits contain anomalous ore-forming elements and pathfinders indicating the presence of concealed ore deposits. For example, the content distributions of ore-forming elements and pathfinders (e.g., Zn, Cu, Sb, and Pb) in geogas and soil along Prospecting Line 20 in the Jiaolongzhang Pb-Zn deposit are highly consistent [111]. This may be due to the relatively shallow burial depth of concealed ore deposits and thin transported cover; here, both geogas and soil geochemical exploration can indicate the presence of concealed ore deposits well. The same result is also seen in geogas and soil along Prospecting Line 15 above the concealed ore deposits of the Wangjiazhuang Cu deposit [88,89]. Unlike the previous case, geogas and soil geochemical anomalies are present over the concealed ore deposits, but their locations are not consistent in some deposits, for example, the Dongji Au deposit and Dongshan Pb-Zn deposit in Yunnan Province [72,92].

The second scenario appears in areas with a transported overburden. Traditional soil geochemical surveys have failed to reveal such concealed ore deposits; however, geogas surveys provide compelling evidence for locating concealed ore deposits. The Jiaolongzhang Pb-Zn deposit is covered by loess, and anomalous Cd, Zn, Pb, and Cu contents in geogas samples appear over concealed ore deposits along Prospecting Line 48; in contrast, no geochemical anomalies in the corresponding soils were detected [86]. In the forest marsh area of the Taipinggou Cu-Mo deposit, Lu [59] demonstrated that geogas Mo anomalies without corresponding soil Mo anomalies are valid for targeting concealed ore deposits. In the Jiajika rare metal orefield, significant geogas Li, Be, Rb, Cs, Na, and B anomalies are detected, but no soil geochemical anomalies along Prospecting Line 35 of X03 ore body 30–100 m below the earth's surface are identified [101].

The third scenario appears in areas with ore bodies (or mineralization) outcrops, in which ore-forming elements are highly active under supergene weathering. Ore-forming elements and pathfinders produced by the weathering of outcrops experience long-distance migration and form secondary geochemical anomalies far from primary halos. This has been portrayed in the Taipinggou Cu-Mo deposit because Mo is highly active during supergene weathering [112]. In addition, no consensus on whether surface pollution (e.g., slag and the ore accumulation area) affects geogas-carried metal prospecting is present. Tong et al. [72] suggested that the accumulation of slag on the surface significantly influences geogas anomalies. However, Zhou et al. [74] revealed the absence of the NAMEG anomaly in an area contaminated by the previous stacking of Pb-Zn ores.

The aforementioned comparisons of soil and geogas geochemical surveys are sufficient to portray that ore-forming elements and pathfinders in geogas are derived from concealed ore deposits instead of soils. Additional evidence for this conclusion has been provided by various NAMEG studies. Hu et al. [53] demonstrated that carbon-bearing particles (containing C and metallic elements, e.g., Fe, Zn, Au, Cu, and Pb) in geogas originate exclusively from greater depths instead of soils and contain valuable information about

concealed ore deposits. Wang et al. [113] suggested that NAMEG are smaller in size, have a higher degree of polymerization, and are simpler in composition than soil.

2.4. Influencing Factors of Geogas-Carried Metal Prospecting

Geogas-carried metal prospecting consists of three components: geogas, ore-related NAMEG, and vertical migration. The factors affecting these three parameters may have a significant impact on geogas-carried metal prospecting.

The influencing factors related to geogas include the source, composition, and flux of geogas and the changes in geogas in supergene environments. Geogas is sourced from deep-earth degassing, gases released from ore deposits, weathering, and the barometric pumping of atmospheric gases [80,111,113,114]. Theoretically, it would be very beneficial to geogas-carried metal prospecting if concealed ore deposits could release abundant gases (e.g., CO₂, SO₂, H₂S, Hg, and CH₄) because of a decrease in temperature and pressure or weathering [34–36,43,113]; these gases tend to carry large amounts of ore-related NAMEG from concealed ore deposits. Deep earth degassing is beneficial for exploring concealed ore deposits that are at greater depths. Gases originating from weathering, barometric pumping of atmospheric gases, decomposition of organic material, evaporation, and other processes play an important role in geogas-carried metal prospecting when supergenesis impacts concealed ore deposits.

Geogas undergoes significant changes in supergene environments [115–117]. Some of the geogas compositions dissolve into groundwater in large quantities (e.g., CO₂, H₂S, and SO₂). A part of geogas composition would experience oxidation and reduction. These changes inevitably lead to the desorption of NAMEG, which may result in a relatively high concentration of nanoparticles in groundwater [118–121].

Few studies have been conducted on the adsorption and transport capacity of nanoparticles by geogas with different compositions, and the geogas flux in geogas-carried metal prospecting. However, we can infer that the adsorption and transport capabilities of geogas with different nanoparticle compositions are different.

Various complex factors influence the composition of NAMEG. First, the rocks that geogas flows through contribute to NAMEG; thus, overburden acts as a natural sieve or barrier. The signals of ore-related nanoparticles are significantly weakened if the overburden is thick, low-permeability, and rich in ore-forming elements, which can increase background values. Some NAMEG are trapped in micropores and microfractures or are adsorbed by soils [73,118]. Furthermore, ore-related nanoparticles are highly unstable and can dissociate from geogas to liquid and solid phases, owing to changes in Eh, pH, and other factors.

An important advantage of geogas-carried metal prospecting is that geogas anomalies appear over concealed ore deposits. To realize a vertical migration of geogas, vertical permeable channels above concealed ore deposits must be present. Geogas will migrate laterally along high-permeability channels (e.g., sandstone, unconformity, and faults) if a tight layer is located above the concealed ore body. In this case, geogas anomalies will not appear directly over the concealed ore deposits.

The vertical migration of geogas is further divided into two cases for discussion. In the first case, no tight layers (e.g., mudstone, shale, and limestone) are located above the concealed ore deposits that can inhibit the vertical migration of geogas. The most common scenario is that the concealed ore body is covered by regolith, which is characterized by high porosity and permeability. The other case is characterized by the presence of high-angle faults, vertical fracture zones [7,61,68,69,113,122–125].

In addition, factors influencing geogas-carried metal prospecting include sampling methods, trapping medium, weather, and temperature [12,16,79,82,90,111,126–128]. At present, researchers have adopted an active sampling method with sampling media consisting of aqua regia and foam plastic [11,16,22,82].

3. Discussion

3.1. Formation of Nanometals in the Mineralization Process

With the development of analytical techniques, abundant metal and mineral nanoparticles have been observed in different rocks and ore deposits. Notably, their composition has been quantitatively determined and suggests that various geological and geochemical processes all can form different metal and mineral nanoparticles (Figure 6) [66,129–134].

Adushkin et al. [129] developed a unidimensional and spherically symmetric internally consistent theory to describe the cavitation mechanism of mineral nano- and microspherule formation in hydrothermal fluids. Adushkin et al. [135] further suggested that the dimensions of nano- and microspherules produced by cavitation are primarily dominated by the thermophysical properties of their constituents, instead of the depth of the host rock occurrence. González-Jiménez and Reich [132] observed abundant platinum-group element nanoparticles (PGE-NPs) in the Caridad chromite deposit (eastern Cuba) and suggested that PGE-NPs can form under a wide spectrum of thermal and pressure conditions. Furthermore, aqueous fluids may significantly contribute to producing PGE-NPs during the metamorphism and metasomatism of the chromite deposits. Verdugo-Ihl et al. [133] observed Si-bearing hematite nanoparticle inclusions and Cu and Cu-As nanoparticles, and they concluded that their distribution characteristics indicated fluid–mineral interaction.

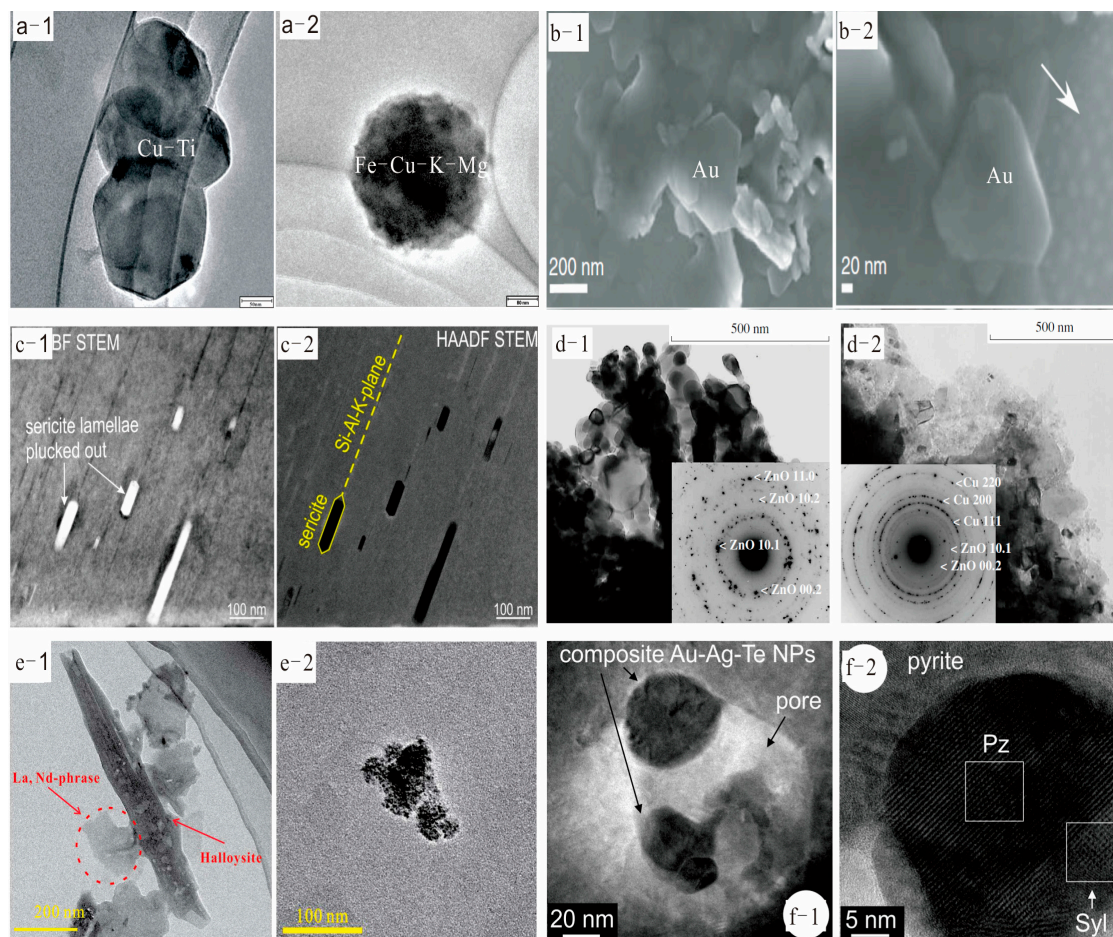


Figure 6. Metal and mineral nanoparticles in different ore deposits. Cu–Ti (a-1) and Fe–Cu–K–Mg (a-2) nanoparticles in ore rocks of Zhou’an Cu–Ni deposit [66,136]; (b-1,b-2) gold nanoparticles in saprokatat the Golden Virgin pit [131]; (c-1,c-2) sericite nanoparticles in rocks of thelympic Dam deposit [133]; ZnO (d-1,d-2) ZnO and Cu nanoparticles in inclusions in the Dukat Ore Field [130]; La–Nd-bearing nanoparticles (e-1,e-2) Ce-bearing nanoparticles in supergene rare earth element mineralization [137], and (f-1,f-2) Au–Ag–Sb nanoparticles in arsenic-free pyrite [138].

More appealing and instructive studies have been conducted on nanoparticles in pyrite from the mineral crystal microstructure perspective. Deditius et al. [139] observed a considerable abundance of various nanoparticles in a matrix of distorted and polycrystalline pyrites from Carlin-type and epithermal deposits. Nanoparticles can be further divided into three groups based on their chemical composition: native metals, sulfides and sulfosalts, and Fe-bearing nanoparticles. They further suggested that the nanoparticles formed by exsolution from the pyrite matrix or by direct precipitation from the hydrothermal solution. Ciobanu et al. [138] first documented the pore-attached composite Au–Te nanoparticles in As-free pyrite and revealed that the Au–Te nanoparticles were indicative of Au-trapping during crustal metamorphism. Li et al. [134] further suggested that gold nanoparticles incorporated into the crystal interface or occasionally the crystal lattice (0.22–0.54 nm) of pyrite, based on a detailed study on auriferous pyrites from the Jiaodong gold deposit, which was significant for visualizing the distribution and aggregation of gold in pyrite.

3.2. Migration in the Secondary Process

Wang et al. [136] categorized ore deposits into seven types. Type A deposits are exposed deposits that can be delineated using traditional litho-geochemical and stream sediment geochemical surveys, and by prospectors with naked eyes, owing to their natural exposure on the Earth's surface. Type B deposits are concealed in host rocks, and primary halos (leakage or diffusion halos) are effective for identifying these geochemical anomalies. Type C deposits are covered by a veneer of residuum, and soil and stream sediment geochemical surveys are useful for their discovery. Type D deposits are entirely covered by exotic transported soils; therefore, traditional soil and stream sediments are not suitable for their identification. Type E deposits are concealed by various post-mineralization covers (e.g., volcanic and sedimentary rocks, alluvium, and weathered cover). Type F deposits are hosted at the bottom of volcanic rocks, above which the transported cover is well-developed. Type G deposits are hosted by sedimentary rocks (Figure 7). Type D, E, F, and G deposits are challenging to detect using conventional rock, soil, and stream sediment geochemical methods, which are generally practiced. A schematic of the NAMEG characteristics of the seven types of ore deposits is shown in Figure 7. The use of geogas-carried metal prospecting is not required in the geochemical exploration of type A, B, or C deposits, because traditional and economical rock, soil, and stream sediment geochemical surveys are effective for discovering these deposits.

Detailed demonstrations of the genesis of NAMEG anomalies over type D, E, F, and G deposits were conducted individually (Figure 8).

Type D deposits are most commonly investigated for geogas-carried metal prospecting. NAMEG, along with geogas, migrate vertically through permeable regolith, thus forming NAMEG anomalies over concealed ore deposits [6,85,136,140]. Ascending geogas flows are derived from the barometric pumping of atmospheric gases, gases released from ore deposits, and deep-earth degassing; among them, gases released from ore deposits may be dominant. The weathering of ore deposits may emancipate and form abundant nanoscale metals [64,131,141–144], which is vital for the formation of strong NAMEG anomalies over concealed ore deposits (Figure 8). The permeable regolith allows for the free vertical migration of nanoscale metals and geogas; that is, there are no low-permeability layers (e.g., mudstone and shale) above concealed ore deposits. Otherwise, nanoscale metals and geogas migrate laterally rather than vertically along permeable channels (e.g., permeable sandstone, regolith, faults, and fractures). In addition, a thick regolith is not conducive to the formation of strong NAMEG anomalies above the concealed ore deposits. Nanoscale metals undergo oxidation, reduction, adsorption, and other geochemical processes that lead to their retention in soil [54,62,145–148].

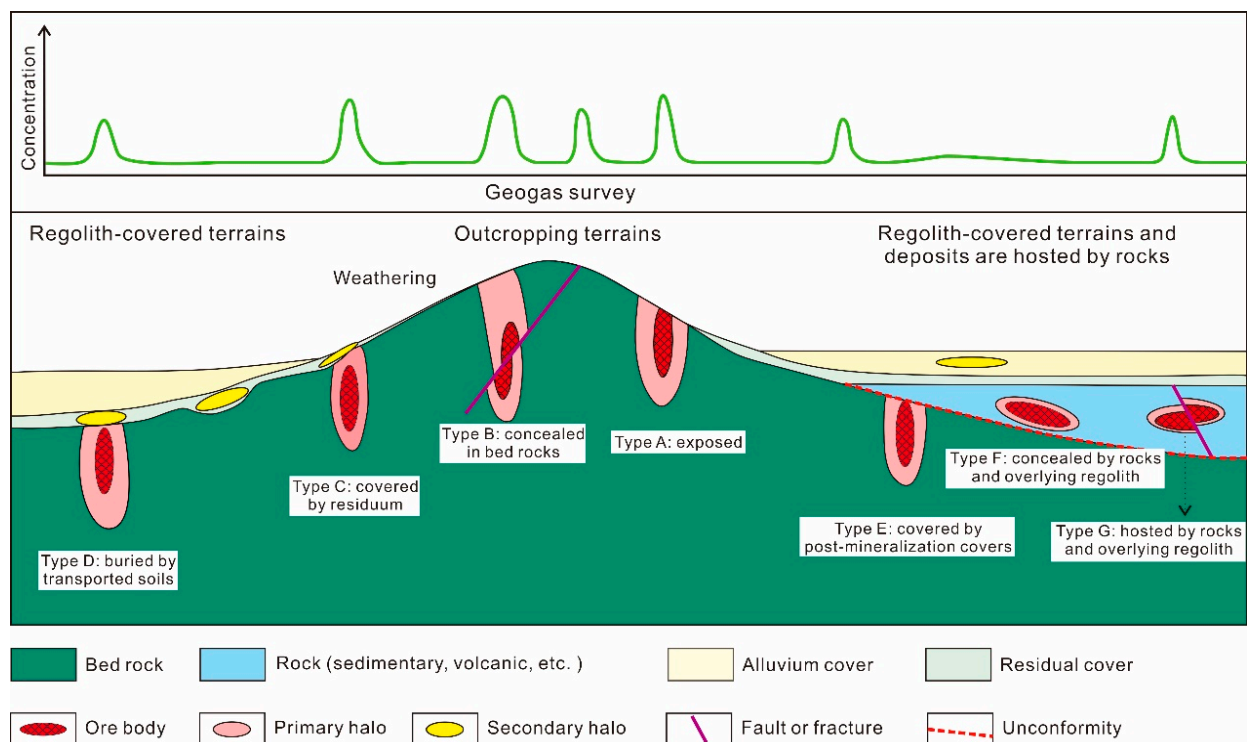


Figure 7. Schematic diagram showing the seven occurrence types of ore deposits and corresponding geogas anomaly characteristics (Modified after Wang et al. [136]).

The overburdens in type E deposits consist of low-permeability rocks (e.g., volcanic and sedimentary rocks) and permeable regolith. In addition, an unconformity exists between the bedrock and the overburdens. Unconformities are perfect transportation channels for geogas [148–150]. Nanoscale metals carried by geogas first migrate laterally along the unconformity and, subsequently, vertically through the regolith. Therefore, strong NAMEG anomalies appear where the low-permeability layer pinches out on the surface. There are weak or no NAMEG anomalies over the concealed ore deposits (Figure 8).

Both type F and G deposits are characterized by low-permeability rocks above them. In these scenarios, permeable channels such as faults and fractures related to the ore body are vital for forming NAMEG anomalies. The locations of the NAMEG anomalies appear directly over the concealed ore deposits and elsewhere, depending on the occurrence of faults and fracture zones (Figure 8). Otherwise, weak or no geochemical anomalies are detected over the concealed ore deposits. Faults (or fractures) play a vital role in the formation of NAMEG anomalies over concealed ore deposits with low-permeability overburdens. Faults (or fractures) are preferential geogas migration pathways because they represent permeability-enhanced zones [7,61,68,69,113,123–125,151]. More potent evidence for the migration of nanoscale metals carried by geogas or themselves along faults (or fractures) is provided by transmission electron microscopy and scanning electron microscopy studies of fault gouges. Researchers have observed abundant nanoscale ore-forming particles in fault gouges in different ore deposits (e.g., Shanggong gold deposit, Bairendaba Polymetallic Deposit, and Kaxiutata iron deposit) [53,66,68,69,116,152–157]. Combined with abundant nanoscale metals in ore rocks and geogas [18,21,62–64,66,68,69,135,144,157], they provide in-depth evidence for the genetic mechanism of the NAMEG method.

In addition, as summarized by Anand et al. [158], many mechanisms contribute to the upward transportation of ore-related metals through exotic covers. Therefore, covers over concealed ore deposits tend to have certain amounts of ore-related metals, which may also contribute to NAMEG. For example, gold grains and ionic gold can be transformed into gold

nanoparticles with the involvement of organic matter and microorganisms [62,64,159,160]. Reith et al. [62] even consider biofilms living on Au grains as effective nanoparticle factories that promote the dispersion of Au via the formation of Au nanoparticles.

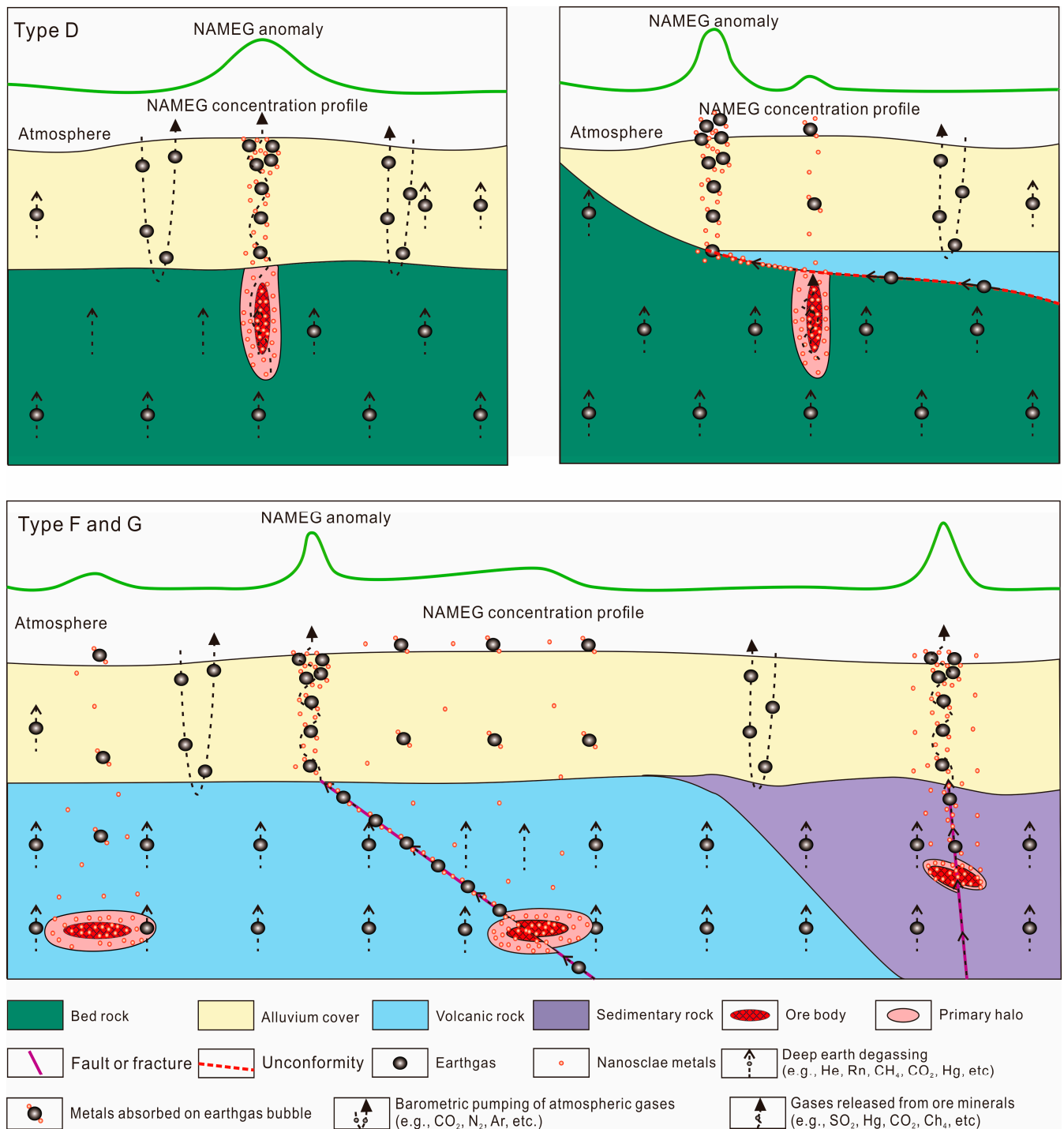


Figure 8. Schematic diagram showing the genesis of NAMEG anomaly for concealed ore deposits in regolith-covered terrains (Note: arrows represent the direction of geogas migration).

Geochemical anomalies can nevertheless form over concealed ore deposits when low-permeability rocks reside above them. However, such geochemical anomalies are so weak that both artificial and natural factors may render them meaningless.

3.3. Application Effectiveness

3.3.1. Different Types of Ore Deposits

Theoretically, geogas transports ore-related nanoparticles to the surface to form geochemical anomalies when they flow through concealed ore deposits. Statistics have compiled the current successful applications based on ore-forming elements (Figure 9). The results showed that geogas-carried metal prospecting is a potentially effective tool for the exploration of Cu, Au, Zn, Pb, U, Sn, and Ag ore deposits. Only a few case studies have been conducted on Fe and W ore deposits. The well-known Jiajika superlarge Li-polymetallic deposit in western Sichuan is an exclusive example of a study on rare metal ore deposits. On Prospecting Line 35 of the X03 ore body, continuous geogas anomalies of Li, Be, Rb, Cs, Na, and B are present over two deposits at depths of 30–100 m, which are not accompanied by any soil geochemical anomalies [101]. Notably, the ore-forming elements in the Jiajika superlarge Li-polymetallic deposit include Li, Be, Nb, Ta, or Sn [161,162], but the geogas shows no Nb, Ta, or Sn anomalies. This suggests, to some extent, that not all ore-forming elements can appear as geogas anomalies over concealed ore deposits.

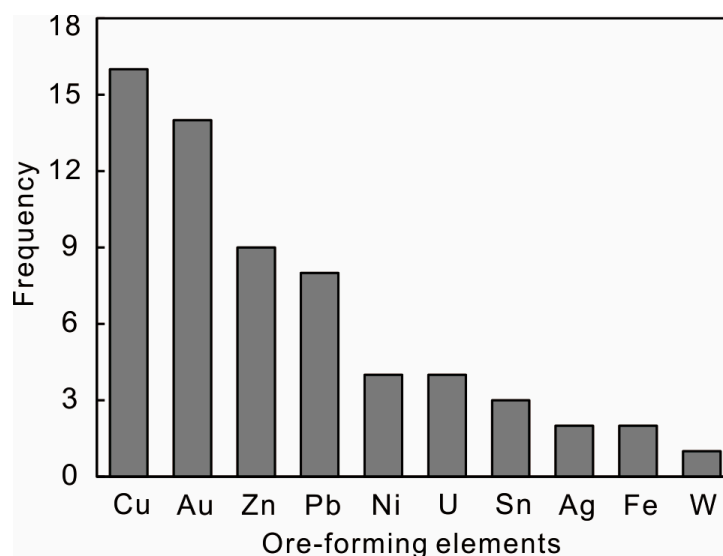


Figure 9. A statistical histogram of successful case studies of geogas-carried metal prospecting based on ore-forming elements.

From the perspective of the genetic type of the deposit, most successful case studies (Cu, Zn, Pb, Ni, Ag, and Fe) belong to magma-related metal sulfide deposits and hydrothermal deposits, indicating that geogas-carried metal prospecting is a quite useful tool for the exploration of such deposits. The only example of a sedimentary deposit is the Dongshengmiao polymetallic pyrite deposit, which is a submarine exhalation sedimentary/weakly reformed type [163]. Currently, the applicability of geogas-carried metal prospecting to different ore deposits is limited. Elemental geochemical behavior may have an impact on the effectiveness of geogas-carried metal prospecting. More efforts are needed to verify the effectiveness of geogas-carried metal prospecting for other types of ore deposits with various ore metals (e.g., ion-adsorption rare-earth ore deposits and paleo-weathering crust sedimentary type deposits).

3.3.2. Different Geochemical Landscapes and Climates

Different geochemical landscapes are characterized by distinct geological backgrounds, climates, vegetation development, and covers, all of which may affect the effectiveness of geogas-carried metal prospecting. The Chinese landscape division suitable for geochemical exploration was adopted to demonstrate the applicability of geogas-carried metal prospecting in different geochemical landscapes (Figure 10) [164,165].

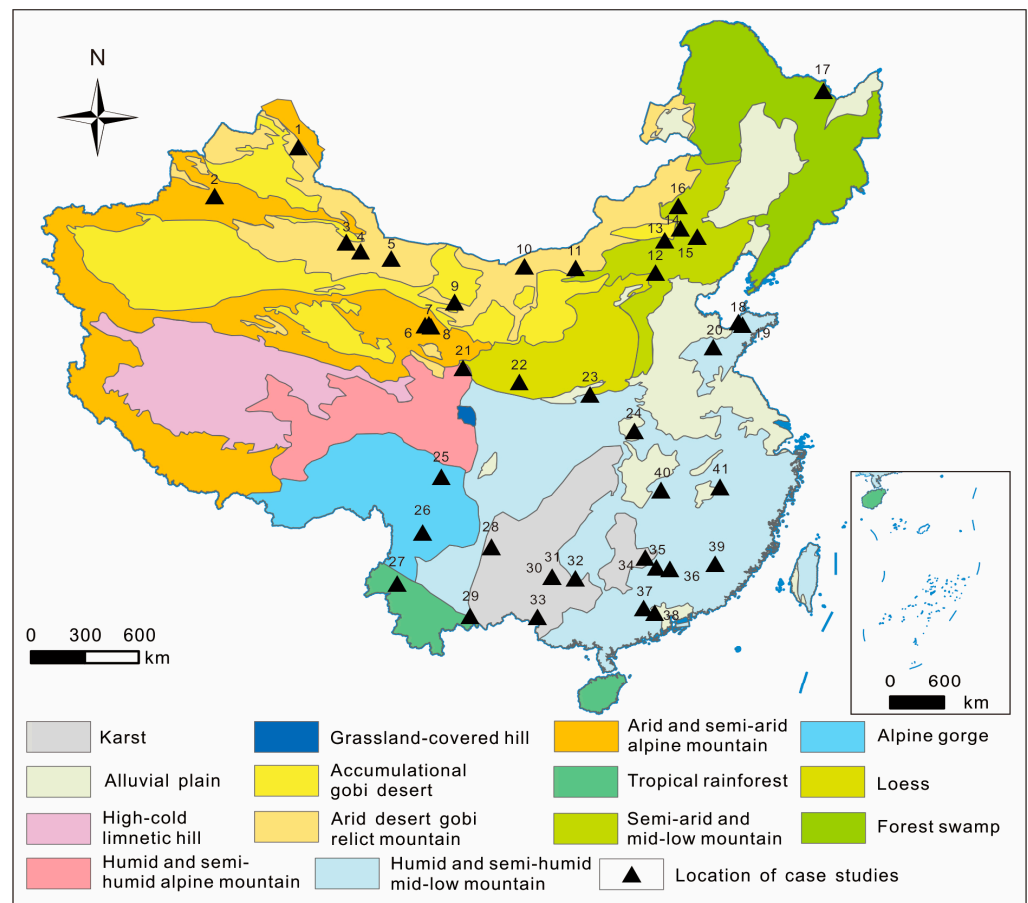


Figure 10. Distribution map of the case studies of geogas-carried metal prospecting in different geochemical landscapes in China: 1—Salbulack Au deposit, 2—W-Sn polymetallic ore deposit, 3—Jinwozi 210 gold deposit, 4—Tianyu Cu-Ni deposit, 5—Gongpoquan porphyry Cu deposit, 6—deposits in Beiqilian area, 7—deposits in Heihe Basin, 8—deposits in Gadaban district, 9—Kaxiutata iron deposit, 10—Dongshengmiao polymetallic pyrite deposit, 11—Laoyanghao gold ore district, 12—Zhangquanzhuang gold district, 13—Budunhua copper deposit, 14—Hongshanzi uranium prospecting area, 15—Chaihulanzi gold deposit, 16—Bairendaba lead-zinc deposit, 17—Tuanjiogou gold deposit, 18—Dayinggezhuang gold deposit, 19—Dongji gold deposit, 20—Wangjiazhuang copper deposit, 21—Lashuixia Cu-Ni deposit, 22—Jiaolongzhang Pb-Zn deposit, 23—Shengjiayao gold deposit, 24—Zhou’an Cu-Ni deposit, 25—Jiajika rare metal ore field, 26—Mofancun prospecting area, 27—Dongshan Pb-Zn deposit, 28—Tongchanghe copper mine, 29—Kafang copper deposit, 30—Zn-Cu deposit in Dachang area, 31—Dachang Sn polymetallic ore deposit, 32—Qingmingshan Cu-Ni sulfide deposit, 33—Debao copper deposit, 34—Fankou lead-zinc deposit, 35—Huangshaping-Liaojiawan Ag-Pb-Zn polymetallic ore deposit, 36—Renhua uranium exploration area, 37—Hetai ore district, 38—Changkeng gold deposit, 39—Yueyang Ag-Au deposit, 40—Lijiaduan uranium deposit, and 41—Yuxing copper deposit (landscape was modified after Guo et al. [164] and Liu et al. [165]).

Geochemical landscapes with successful field experiments and applications of geogas-carried metal prospecting include karsts, the Gobi Desert, swamps and forest, loesses, humid hills, humid cold mountains, alluvial plains, rainforests, arid hills, arid cold mountains, and canyons. Among them, only one successful case study exists in the alluvial plain and forest swamp landscapes, suggesting that the effectiveness of geogas-carried metal prospecting in such terrain is questionable. Therefore, more field experiments and applications should be conducted for geogas-carried metal prospecting in these two geochemical landscapes.

Geochemical landscapes with no successful field experiments and applications of geogas-carried metal prospecting comprise hilly grassland, deserts, and cold swamps.

Research on the applicability of geogas-carried metal prospecting in hilly grassland has little significance, due to its limited area in China. The desert landscape primarily consists of desert basins (e.g., the Junggar, Tarim, and Qaidam basins). These desert basins are characterized by thick transported covers that comprise various formations with different permeabilities (e.g., permeable sandstone and low-permeability mudstone). The presence of low-permeability rocks likely impedes the vertical transport of geogas and further weakens the effectiveness of geogas-carried metal prospecting. Cold swamp is a typical geochemical landscape in western China and is characterized by aeolian sand accumulation, which may greatly interfere with geochemical exploration [166,167]. Further research should be conducted to demonstrate the effectiveness of geogas-carried metal prospecting in cold swamp landscapes, because this method can potentially exclude the influence of aeolian sands. Another issue that should be considered is the presence of permafrost in cold swamp landscapes [168,169], which may act as a barrier during the vertical migration of geogas.

4. Conclusions and Outlook

Our conclusions are as follows:

(1) Geogas originates from deep-earth degassing, gases released by ore deposits, and the barometric pumping of atmospheric gases. Additional research is required to quantitatively determine the exact gas source and composition that serve as the dominant carrier gas.

(2) NAMEG vary in size, shape, composition, and structure. Subsequent work should be carried out to determine whether NAMEG characteristics can provide useful information on concealed ore deposits.

(3) Field experiments and applications in China conclude that geogas-carried metal prospecting is a useful tool for the exploration of concealed ore deposits with burial depths of >800 m in various climate zones and geochemical landscapes, and possible genetic models of NAMEG anomalies were constructed.

(4) Magmatic and hydrothermal deposits are the primary ore types in which geogas-carried metal prospecting has been successfully carried out. Further investigating the applicability of geogas-carried metal prospecting for special ore types and geochemical landscapes is required.

Author Contributions: Conceptualization, Q.W., X.W., Z.C., B.Z. and H.L.; validation, Z.D., T.Y. and H.Y.; writing—original draft preparation, Q.W. and X.W.; writing—review and editing, Q.W., X.W. and H.L.; supervision, X.L., Z.C. and Y.Q. All authors have read and agreed to the published version of the manuscript.

Funding: This study is jointly supported by the National Key Research and Development Plan (Grant No. 2023YFC2906405), the Joint Funds of the National Natural Science Foundation of China (Grant No. U2244219), the Foundation Project of the Chinese Academy of Geological Sciences (Grant No. JKYZD202327), and Chemical Earth (Grant No. GEO WP23_35 and UNESCO 37/33).

Data Availability Statement: Not applicable.

Conflicts of Interest: Y.Q. is employees of Zijin Mining Group Co., Ltd. The paper reflects the views of the scientist and not the company. The remaining authors declare that the research was conducted in the absence of any commercial or financial relationships that could be construed as a potential conflict of interest.

References

1. Xie, X.J. Tactical and strategic deep-penetration geochemical surveys. *Earth Sci. Front.* **1998**, *5*, 171–183. (In Chinese with English Abstract)
2. Wang, X.Q. Deep penetration exploration geochemistry. *Geophys. Geochem. Explor.* **1998**, *22*, 166–169. (In Chinese with English Abstract)
3. Cameron, E.M.; Leybourne, M.I.; Kelley, D.L. Exploring for deeply covered mineral deposits: Formation of geochemical anomalies in northern Chile by earthquake-induced surface flooding of mineralized groundwaters. *Geology* **2002**, *30*, 1007–1010. [[CrossRef](#)]

4. Cameron, E.M.; Hamilton, S.M.; Leybourne, M.I.; Hall, G.E.; McClenaghan, M.B. Finding deeply buried deposits using geochemistry. *Geochem. Explor. Environ. Anal.* **2004**, *4*, 7–32. [[CrossRef](#)]
5. Xie, X.J.; Wang, X.Q. Recent developments on deep-penetrating geochemistry. *Earth Sci. Front.* **2003**, *10*, 225–238. (In Chinese with English Abstract)
6. Kristiansson, K.; Malmqvist, L. Evidence for nondiffusive transport of ^{222}Rn in the ground and a new physical model for the transport. *Geophysics* **1982**, *47*, 1444–1452. [[CrossRef](#)]
7. Kristiansson, K.; Malmqvist, L.; Persson, W. Geogas prospecting: A new tool in the search for concealed mineralizations. *Endeavour* **1990**, *14*, 28–33. [[CrossRef](#)]
8. Krčmar, B. Method of Elements' Molecular Form Capture in Atmospheric Air Emitted by Geological Structures. Czech Republic Patent No. 268641, 25 November 1988.
9. Klusman, R.W. *Soil Gas and Related Methods for Natural Resource Exploration*; John Wiley & Sons: Hoboken, NJ, USA, 1993; pp. 1–473.
10. Wang, X.Q.; Cheng, Z.Z.; Lu, Y.X.; Xu, L.; Xie, X.J. Nanoscale metals in earthgas and mobile forms of metals in overburden in wide-spaced regional exploration for giant deposits in overburden terrains. *J. Geochem. Explor.* **1997**, *58*, 63–72. [[CrossRef](#)]
11. Wang, M.Q.; Gao, Y.Y.; Liu, Y.H. Progress in the collection of Geogas in China. *Geochem. Explor. Environ. Anal.* **2008**, *8*, 183–190. [[CrossRef](#)]
12. Gao, Y.Y.; Wang, M.Q.; Zhang, D.E. Application of 'metals-in-soil-gas' techniques to mineral exploration in exotic overburden. *Geochem. Explor. Environ. Anal.* **2011**, *11*, 63–70. [[CrossRef](#)]
13. Wang, X.Q. The current situation and future of geogas. *Foreign Geoexplor. Tech.* **1996**, 12–18. (In Chinese with English Abstract)
14. Kristiansson, K.; Malmqvist, L. The depth-dependence of the concentration of ^{222}Rn in soil gas near the surface and its implication for exploration. *Geoexploration* **1984**, *22*, 17–41. [[CrossRef](#)]
15. Malmqvist, L.; Kristiansson, K. Experimental evidence for an ascending microflow of geogas in the ground. *Earth Planet. Sc. Lett.* **1984**, *70*, 407–416. [[CrossRef](#)]
16. Kristiansson, K.; Malmqvist, L. Trace elements in the geogas and their relation to bedrock composition. *Geoexploration* **1987**, *24*, 517–534. [[CrossRef](#)]
17. Wang, X.Q.; Xie, X.J.; Lu, Y.X. Dynamic collection of geogas and its preliminary application in search for concealed deposits. *Geophys. Geochem. Explor.* **1995**, *22*, 81–89. (In Chinese with English Abstract)
18. Tong, C.H.; Li, J.C.; Ge, L.Q.; Yang, F.G. Experimental observation of the nano-scale particles in geogas matters and its geological significance. *Sci. China Ser. D Earth Sci.* **1998**, *41*, 325–329. [[CrossRef](#)]
19. Wang, X.Q. Conceptual model of deep-penetrating geochemical migration. *Geol. Bull. China* **2005**, *24*, 892–896. (In Chinese with English Abstract)
20. Cao, J.J. A technique for detecting concealed deposits by combining geogas particle characteristics with element concentrations. *Metal Mine* **2009**, 1–4. (In Chinese with English Abstract)
21. Cao, J.J.; Hu, X.Y.; Jiang, Z.T.; Li, H.W.; Zou, X.Z. Simulation of adsorption of gold nanoparticles carried by gas ascending from the Earth's interior in alluvial cover of the middle–lower reaches of the Yangtze River. *Geofluids* **2010**, *10*, 438–446. [[CrossRef](#)]
22. Wang, X.Q.; Ye, R. Findings of nanoscale metal particles: Evidence for deep-penetrating geochemistry. *Acta. Geol. Sin.* **2011**, *32*, 7–12. (In Chinese with English Abstract)
23. Zhang, B.M.; Wang, X.Q.; Ye, R.; Zhou, J.; Liu, H.L.; Liu, D.S.; Han, Z.X.; Lin, X.; Wang, Z.K. Geochemical exploration for concealed deposits at the periphery of the Zijinshan copper–gold mine, southeastern China. *J. Geochem. Explor.* **2015**, *157*, 184–193. [[CrossRef](#)]
24. Du, L.T. Five gas-spheres and hydrogen, hydrocarbon resources in the earth—With a discuss on geodynamics of gas. *Uran. Geol.* **1993**, *9*, 9257–9265. (In Chinese with English Abstract)
25. Dixon, J.E. Degassing of alkalic basalts. *Am. Mineral.* **1997**, *82*, 368–378. [[CrossRef](#)]
26. Sparks, R.S.J. Dynamics of magma degassing. *Geol. Soc. Lond. Spec. Publ.* **2003**, *213*, 5–22. [[CrossRef](#)]
27. Chiodini, G.; Cardellini, C.; Di Luccio, F.; Selva, J.; Frondini, F.; Caliro, S.; Rosiello, A.; Beddini, G.; Ventura, G. Correlation between tectonic CO_2 Earth degassing and seismicity is revealed by a 10-year record in the Apennines, Italy. *Sci. Adv.* **2020**, *6*, eabc2938. [[CrossRef](#)] [[PubMed](#)]
28. Oppenheimer, C.; Fischer, T.P.; Scaillet, B. Volcanic degassing: Process and impact. *Treatise Geochem.* **2014**, *4*, 111–179. [[CrossRef](#)]
29. Kerrick, D.M.; and Caldeira, K. Metamorphic CO_2 degassing from orogenic belts. *Chem. Geol.* **1998**, *145*, 213–232. [[CrossRef](#)]
30. Machel, H.G. Relationships between sulphate reduction and oxidation of organic compounds to carbonate diagenesis, hydrocarbon accumulations, salt domes, and metal sulphide deposits. *Carbonates Evaporites* **1989**, *4*, 137–151. [[CrossRef](#)]
31. Whiticar, M.J.; Suess, E. Hydrothermal hydrocarbon gases in the sediments of the King George Basin, Bransfield Strait, Antarctica. *Appl. Geochem.* **1990**, *5*, 135–147. [[CrossRef](#)]
32. Polito, P.A.; Clarke, J.D.A.; Bone, Y.; Viellenave, J. A CO_2 - O_2 -light hydrocarbon-soil gas anomaly above the Junction orogenic gold deposit: A potential, alternative exploration technique. *Geochem. Explor. Environ. Anal.* **2002**, *2*, 333–344. [[CrossRef](#)]
33. Conrad, R. Soil microorganisms as controllers of atmospheric trace gases (H_2 , CO , CH_4 , OCS , N_2O , and NO). *Microbiol. Rev.* **1996**, *60*, 609–640. [[CrossRef](#)] [[PubMed](#)]

34. Hinkle, M.E.; Ryder, J.L.; Sutley, S.J.; Botinelly, T. Production of sulphur gases and carbon dioxide by synthetic weathering of crushed drill cores from the Santa Cruz porphyry copper deposit near Casa Grande, Pinal County, Arizona. *J. Geochem. Explor.* **1990**, *38*, 43–67. [[CrossRef](#)]
35. Reid, A.D.; Rasmussen, J.D. The use of soil gas CO₂ in the exploration for sulphide bearing breccias pipes in northern Arizona. *J. Geochem. Explor.* **1990**, *38*, 87–101. [[CrossRef](#)]
36. Plet, C.; Siegel, C.; Woltering, M.; Noble, R.; Pagès, A.; Thorne, R.; Spinks, S.; and Anand, R. Sulfur and CO₂ gases emitted during weathering of sulfides: Role of microbial activity and implications to exploration through cover. *Ore Geol. Rev.* **2021**, *134*, 104167. [[CrossRef](#)]
37. Nilson, R.H.; Peterson, E.W.; Lie, K.H.; Burkhard, N.R.; Hearst, J.R. Atmospheric pumping: A mechanism causing vertical transport of contaminated gases through fractured permeable media. *J. Geophys. Res.-Sol. Earth* **1991**, *96*, 21933–21948. [[CrossRef](#)]
38. Carrigan, C.R.; Hudson, G.B.; Nitao, J.J.; Zucca, J.J.; Heinle, R.A. Trace gas emissions on geological faults as indicators of underground nuclear testing. *Nature* **1996**, *382*, 528–531. [[CrossRef](#)]
39. McCarthy, J.H. Mercury vapor and other volatile components in the air as guides to ore deposits. *J. Geochem. Explor.* **1972**, *1*, 143–162. [[CrossRef](#)]
40. Boyle, R.W.; Jonasson, I.R. The geochemistry of arsenic and its use as an indicator element in geochemical prospecting. *J. Geochem. Explor.* **1973**, *2*, 251–296. [[CrossRef](#)]
41. Taylor, C.H.; Kesler, S.E.; Cloke, P.L. Sulfur gases produced by the decomposition of sulfide minerals: Application to geochemical exploration. *J. Geochem. Explor.* **1982**, *17*, 165–185. [[CrossRef](#)]
42. Hale, M. Gas geochemistry and deeply buried mineral deposits: The contribution of the applied geochemistry research group, imperial college of science and technology, London. *Geochem. Explor. Environ. Anal.* **2010**, *10*, 261–267. [[CrossRef](#)]
43. Lin, C.G.; Cheng, Z.Z.; Chen, X.; Lü, Z.C.; Pang, Z.S.; Xue, J.L.; Tao, W. Application of multi-component gas geochemical survey for deep mineral exploration in covered areas. *J. Geochem. Explor.* **2021**, *220*, 106656. [[CrossRef](#)]
44. Dyck, W. The use of helium in mineral exploration. *J. Geochem. Explor.* **1976**, *5*, 3–20. [[CrossRef](#)]
45. Gingrich, J.E. Radon as a geochemical exploration tool. *J. Geochem. Explor.* **1984**, *21*, 19–39. [[CrossRef](#)]
46. McCarthy, J.H.; Reimer, G.M. Advances in soil gas geochemical exploration for natural resources: Some current examples and practices. *J. Geophys. Res. Sol. Earth* **1986**, *91*, 12327–12338. [[CrossRef](#)]
47. Awadh, S.M.; Ali, K.K.; Alazzawi, A.T. Geochemical exploration using surveys of spring water, hydrocarbon and gas seepage, and geobotany for determining the surface extension of Abu-Jir Fault Zone in Iraq: A new way for determining geometrical shapes of computational simulation models. *J. Geochem. Explor.* **2013**, *124*, 218–229. [[CrossRef](#)]
48. Cao, J.J.; Hu, R.Z.; Liang, Z.R.; Peng, Z.L. TEM observation of geogas-carried particles from the Changkeng concealed gold deposit, Guangdong Province, South China. *J. Geochem. Explor.* **2009**, *101*, 247–253. [[CrossRef](#)]
49. Cao, J.J.; Liu, C.; Xiong, Z.H.; Qin, T.R. Particles carried by ascending gas flow at the Tongchanghe copper mine, Guizhou Province, China. *Sci. China Earth Sci.* **2010**, *53*, 1647–1654. [[CrossRef](#)]
50. Wei, X.J.; Cao, J.J.; Holub, R.F.; Hopke, P.K.; Zhao, S.J. TEM study of geogas-transported nanoparticles from the Fankou lead-zinc deposit, Guangdong Province, South China. *J. Geochem. Explor.* **2013**, *128*, 124–135. [[CrossRef](#)]
51. Dai, D.L.; Cao, J.J.; Lai, P.X.; Wu, Z.Q. TEM study on particles transported by ascending gas flow in the Kaxiutata iron deposit, Inner Mongolia, North China. *Geochem. Explor. Environ. Anal.* **2015**, *15*, 255–271. [[CrossRef](#)]
52. Luo, S.Y.; Cao, J.J.; Yan, H.B.; Yi, J. TEM observations of particles based on sampling in gas and soil at the Dongshengmiao polymetallic pyrite deposit, Inner Mongolia, northern China. *J. Geochem. Explor.* **2015**, *158*, 95–111. [[CrossRef](#)]
53. Hu, G.; Cao, J.J.; Hopke, P.K.; Holub, R.F. Study of carbon-bearing particles in ascending geogas flows in the Dongshengmiao polymetallic pyrite deposit, Inner Mongolia, China. *Resour. Geol.* **2015**, *65*, 13–26. [[CrossRef](#)]
54. Wang, X.Q.; Zhang, B.M.; Lin, X.; Xu, S.F.; Ye, R. Geochemical challenges of diverse regolith-covered terrains for mineral exploration in China. *Ore Geol. Rev.* **2016**, *73*, 417–431. [[CrossRef](#)]
55. Li, D.W.; Cao, J.J.; Ke, H.L.; Liu, C.; Wei, X.J. Study of particles from the Kafang copper deposit in Gejiu city, Yunnan. *Geochem. Explor. Environ. Anal.* **2017**, *17*, 367–377. [[CrossRef](#)]
56. Li, Y.K.; Cao, J.J.; Chen, J.; Yi, J. The research of particles carried by ascending gas flow from Qingmingshan Cu-Ni sulfide deposit in Guangxi Province. *Acta Petrol. Sin.* **2017**, *33*, 831–842. (In Chinese with English Abstract)
57. Cao, J.J.; Li, Y.K.; Liu, C.; Yuan, X.L. Research on geogas particles from Bingba copper deposit in Guanling county of Guizhou province. *J. Jilin Univ. (Earth Sci. Ed.)* **2017**, *7*, 95–105. (In Chinese with English Abstract)
58. Lu, M.; Ye, R.; Zhang, B.M.; Yao, W.S.; Han, Z.X. Occurrence and formation of metallic nanoparticles over the concealed ore deposits. *J. Nanosci. Nanotechnol.* **2017**, *17*, 6077–6082. [[CrossRef](#)]
59. Lu, M.; Ye, R.; Wang, Z.K.; Wang, X.J. Geogas prospecting for buried deposits under loess overburden: Taking Shenjiayao gold deposit as an example. *J. Geochem. Explor.* **2019**, *197*, 122–129. [[CrossRef](#)]
60. Jiang, T.; Cao, J.J.; Wu, Z.Q.; Wu, Y.F.; Zeng, J.N.; Wang, Z.H. A TEM study of particles carried by ascending gas flows from the Bairendaba lead-zinc deposit, Inner Mongolia, China. *Ore Geol. Rev.* **2019**, *105*, 18–27. [[CrossRef](#)]
61. Cao, J.J.; Liu, C.; Zhang, P.; Li, Y.P.; Xiong, Z.H. The characteristic of geogas particles from Daheishan Basalt Copper Deposit in Huize County of Yunnan. *Metal Mine* **2011**, *6*, 113–115. (In Chinese with English Abstract)
62. Reith, F.; Fairbrother, L.; Nolze, G.; Wilhelmi, O.; Clode, P.L.; Gregg, A.; Parsons, J.E.; Wakelin, S.A.; Pring, A.; Hough, R.; et al. Nanoparticle factories: Biofilms hold the key to gold dispersion and nugget formation. *Geology* **2010**, *38*, 843–846. [[CrossRef](#)]

63. Cao, J.J. Migration mechanisms of gold nanoparticles explored in geogas of the Hetai ore district, southern China. *Geochem. J.* **2011**, *45*, 9–13. [[CrossRef](#)]
64. Hough, R.M.; Noble, R.R.P.; Reich, M. Natural gold nanoparticles. *Ore Geol. Rev.* **2011**, *42*, 55–61. [[CrossRef](#)]
65. Wang, X.Q.; Zhang, B.M.; Ye, R. Nanogeochemistry for mineral exploration through covers. *Bull. Mineral. Petrol. Geochem.* **2012**, *35*, 43–51. (In Chinese with English Abstract)
66. Wang, X.Q.; Zhang, B.M.; Ye, R. Nanoparticles observed by TEM from gold, copper-nickel and silver deposits and implications for mineral exploration in covered terrains. *J. Nanosci. Nanotechnol.* **2017**, *17*, 6014–6025. [[CrossRef](#)]
67. Gamaletsos, P.N.; Godelitsas, A.; Kasama, T.; Church, N.S.; Douvalis, A.P.; Göttlicher, J.; Steininger, S.; Boubnov, F.; Pontikes, Y.; Tzamos, E.; et al. Nano-mineralogy and-geochemistry of high-grade diasporic karst-type bauxite from Parnassos-Ghiona mines, Greece. *Ore Geol. Rev.* **2017**, *84*, 228–244. [[CrossRef](#)]
68. Zhang, B.M.; Han, Z.X.; Wang, X.Q.; Liu, H.L.; Wu, H.; Feng, H. Metal-bearing nanoparticles observed in soils and fault gouges over the Shenjiayao gold deposit and their significance. *Minerals* **2019**, *9*, 414. [[CrossRef](#)]
69. Han, Z.X.; Zhang, B.M.; Wu, H.; Liu, H.L.; Qiao, Y.; Zhang, S.K. Microscopic characterisation of metallic nanoparticles in ore rocks, fault gouge and geogas from the Shanggong gold deposit, China. *J. Geochem. Explor.* **2020**, *217*, 106562. [[CrossRef](#)]
70. Ju, Y.W.; Li, X.; Ju, L.T.; Feng, H.Y.; Tan, F.Q.; Cui, Y.S.; Yang, Y.; Wang, X.Q.; Cao, J.J.; Qiao, F.; et al. Nanoparticles in the Earth surface systems and their effects on the environment and resource. *Gondwana Res.* **2022**, *110*, 370–392. [[CrossRef](#)]
71. Lu, M.Q.; Cao, J.J.; Hu, G.; Wang, Z.Y.; Ma, S.T. Widespread nearly or nanoscale natural amorphous particles in critical zones from ore deposits. *Ore Geol. Rev.* **2023**, *157*, 105454. [[CrossRef](#)]
72. Tong, C.H.; Liang, X.Z.; Li, J.C. The tentative geogas survey in the Dongji gold deposit. *Geophys. Geochem. Explor.* **1992**, *16*, 445–451. (In Chinese with English Abstract)
73. Wang, M.Q.; Gao, Y.Y. Tracing source of geogas with lead isotopes: A case study in Jiaolongzhang Pb-Zn deposit, Gansu province. *Geochimica* **2007**, *36*, 391–399. (In Chinese with English Abstract)
74. Zhou, S.C.; Liu, X.H.; Tong, C.H.; Hu, B. Application research of geogas survey in prospecting concealed ore. *Acta Geol. Sin.* **2014**, *88*, 736–754. (In Chinese with English Abstract)
75. Zhang, B.M.; Wang, X.Q.; Xu, S.F.; Yao, W.S.; Ye, R. Models and case history studies of deep—penetrating geochemical exploration for concealed deposits in basins. *Geol. China* **2016**, *43*, 1697–1709. (In Chinese with English Abstract)
76. Tong, C.H.; Liang, X.C.; Li, J.C.; Li, G.D. Geogas anomalies on a hidden gold deposit. *Chin. Sci. Bull.* **1991**, *36*, 791–792.
77. Tong, C.H.; Li, J.C. Geogas prospecting and its mechanism in the search for deep seated or concealed gold deposits. *Chin. J. Geophys.* **1999**, *42*, 135–142. (In Chinese with English Abstract)
78. Yin, B.C.; Wu, Z.H.; Jin, Y.F. Geogas aerosol survey: A new method and technique for prospecting concealed ore deposits and studying the geology of structures at depth. *Geol. Geochem* **1997**, 25–30. (In Chinese with English Abstract)
79. Shi, C.Y.; Zhang, J.H.; Liu, Y.H.; Huang, X.M.; Huang, Z.F. Some test results of geogas survey in the Laoyanghao gold ore district, Inner Mongolia. *Geophys. Geochem. Explor.* **1997**, *21*, 247–253. (In Chinese with English Abstract)
80. Wu, Z.H.; Jin, Y.F.; Gu, P. Principles of geogas survey and its application in geological exploration. *Geophys. Geochem. Explor.* **1996**, *20*, 259–264. (In Chinese with English Abstract)
81. Teng, Y.G.; Ni, S.J.; Zhang, C.J.; Tuo, X.G.; Tong, C.H. Making use of geogas, XRF, radon detection to distinguish mineralization of structure in gold ore deposit: Taking Axi and Tianwan gold deposits in Sichuan province for example. *Earth Sci. J. China Univ. Geosci.* **2001**, *26*, 627–630. (In Chinese with English Abstract)
82. Tang, J.R.; Yang, Z.F.; Wang, M.Q.; Liu, Y.Q. Method and application of geogas measurements. *Geophys. Geochem. Explor.* **2004**, *28*, 193–198. (In Chinese with English Abstract)
83. Gao, Y.G.; Yang, Z.F.; Wang, M.Q.; Liu, L.H.; Liu, Y.Q.; Tang, J.R.; Guo, L. Geogas reconnaissance technique in the search for concealed deposits in middle-shallow cover area, Heihe downfaulted basin, Qinghai. *Geol. Prosp.* **2005**, *41*, 73–77. (In Chinese with English Abstract)
84. Wang, M.Q.; Gao, Y.Y.; Zhang, D.E.; Ren, T.X.; Liu, Y.H. Breakthrough in mineral exploration using geogas survey in the basin area of northern Qilian region and its significance. *Geophys. Geochem. Explor.* **2006**, *30*, 7–12. (In Chinese with English Abstract)
85. Gao, Y.Y.; Wang, M.Q.; Xia, X.Z.; Wang, T. Geogas tests in the exploration of concealed metallic deposits in some landscape areas. *Geophys. Geochem. Explor.* **2010**, *34*, 144–149. (In Chinese with English Abstract)
86. Wan, W.; Wang, M.Q.; Gao, Y.Y.; Fan, H.H. Tracing the source of metals in geogas from metal deposits in a loess-covered region. *Bull. Mineral. Petrol. Geochem.* **2016**, *35*, 1290–1297. (In Chinese with English Abstract)
87. Shen, Y.S.; Ma, X.H.; Zhang, Y.J.; Yan, L.B.; Wang, Q.M. Discussion on the anomaly characteristics of Lashuixia Cu-Ni deposit in Qinghai by geogas and mercury gas measurement. *Gold Sci. Technol.* **2009**, *17*, 54–57. (In Chinese with English Abstract)
88. Gao, Y.Y.; Wang, M.Q.; Xia, X.Z.; Wang, T. Results of geogas test in exploring blind metallic deposits in alluvial plain. *Contrib. Geol. Miner. Resour. Res.* **2011**, *26*, 345–349. (In Chinese with English Abstract)
89. Wan, W.; Wang, M.Q.; Hu, M.Y.; Gao, Y.Y. Identification of metal sources in geogas from the Wangjiazhuang copper deposit, Shandong, China: Evidence from lead isotopes. *J. Geochem. Explor.* **2017**, *172*, 167–173. [[CrossRef](#)]
90. Liu, X.H.; Zhou, S.C.; Tong, C.H.; Hu, B. The method and technique for improving the detection sensitivity of dynamic geogas survey. *Geophys. Geochem. Explor.* **2012**, *36*, 1064–1067. (In Chinese with English Abstract)
91. Hu, B.; Zhou, S.C.; Liu, X.H.; Zhao, C.J.; Bao, X.K. Geogas survey experiment for exploration of concealed polymetallic deposit at great depth. *Geophys. Geochem. Explor.* **2012**, *36*, 1068–1072. (In Chinese with English Abstract)

92. Cen, K.; Liu, X.L.; Peng, Z.; Chen, Y. The Application of the Aerosol Geochemical Exploration Method to the Jinwozi Gold Deposit. *Geophys. Geochem. Explor.* **2014**, *38*, 18–22. (In Chinese with English Abstract)
93. Zhou, S.C.; Liu, X.H.; Bo, H.U. Geological significance of geogas field information. *Geophys. Geochem. Explor.* **2012**, *36*, 1044–1049. (In Chinese with English Abstract)
94. Ding, X.T.; Zhou, S.C.; Zhao, C.J.; Zhao, F.; Liu, G.A.; Liu, J. The geogas and soil geochemical characteristics of Pb-Zn deposit in Dongshan, the western of Yunnan province. *Metal Mine* **2013**, *42*, 95–99. (In Chinese with English Abstract)
95. Liu, C.; Cao, J.J.; Ke, H.L. Geogas characteristic of Yongshengde copper ores in the Northeastern Yunnan, China. *Geol. Chem. Miner.* **2011**, *33*, 201–207. (In Chinese with English Abstract)
96. Liu, Z.; Fang, F.; Sun, S.; Tan, H.T.; Zhang, Z. Hubei li section of uranium anomaly and prospecting foreground analysis. *Sichuan Nonferrous Met.* **2013**, 40–47. (In Chinese with English Abstract)
97. Wang, Y.; Ye, R.; Liu, H.J.; Wu, G.D.; Wang, D.S. Deep-penetrating geochemical microscopic evidence in the hydrothermal uranium deposit exploration. *World Nucl. Geosci.* **2017**, *34*, 167–173. (In Chinese with English Abstract)
98. Liu, Y.H.; Yang, K.; Chen, H.X.; Wang, H.H.; Luo, J.L.; Zhu, H.F. The application and significance of deep prospecting by using geogas survey in Xitian area, Hunan province. *Geophys. Geochem. Explor.* **2018**, *42*, 234–240. (In Chinese with English Abstract)
99. Han, W.; Liu, H.Z.; Wang, C.W.; Song, Y.T.; Wang, Q.L.; Kong, M. Geochemical characteristics and indication significance of geogas survey in the Tianyu Cu-Ni deposit of Hami. *Geophys. Geochem. Explor.* **2019**, *43*, 502–508. (In Chinese with English Abstract)
100. Wan, W.; Wang, M.Q.; Gao, Y.Y.; Qin, H.H.; Lai, D.R. Experimental study of geogas method to prospecting for concealed deposit in red soil regions of the south China. *Contrib. Geol. Miner. Resour. Res.* **2019**, *34*, 438–444. (In Chinese with English Abstract)
101. Wang, Q.B.; Liang, B.; Liu, T.; Xu, Z.Q.; Geng, Y. Detection of concealed ore bodies in Jiajika rare metal orefield using geogas prospecting technology. *Bull. Geol. Sci. Technol.* **2020**, *39*, 85–93. (In Chinese with English Abstract)
102. Reich, M.; Kesler, S.E.; Utsunomiya, S.; Palenik, C.S.; Chrystosoulis, S.L.; Ewing, R.C. Solubility of gold in arsenian pyrite. *Geochim. Cosmochim. Acta* **2005**, *69*, 2781–2796. [[CrossRef](#)]
103. Shuster, J.; Reith, F.; Cornelis, G.; Parsons, J.E.; Parsons, J.M.; Southam, G. Secondary gold structures: Relics of past biogeochemical transformations and implications for colloidal gold dispersion in subtropical environments. *Chem. Geol.* **2017**, *450*, 154–164. [[CrossRef](#)]
104. Shuster, J.; Reith, F. Reflecting on gold geomicrobiology research: Thoughts and considerations for future endeavors. *Minerals* **2018**, *8*, 401. [[CrossRef](#)]
105. Wyatt, M.A.; Johnston, C.W.; Magarvey, N.A. Gold nanoparticle formation via microbial metallophore chemistries. *J. Nanopart. Res.* **2014**, *16*, 2212. [[CrossRef](#)]
106. Reith, F.; Rea, M.A.D.; Sawley, P.; Zammit, C.M.; Nolze, G.; Reith, T.; Rantanen, K.; Bissett, A. Biogeochemical cycling of gold: Transforming gold particles from arctic Finland. *Chem. Geol.* **2018**, *483*, 511–529. [[CrossRef](#)]
107. Xu, Y.; Wang, M.Q.; Gao, Y.Y.; Ouyang, H. Tracing the source of geogas materials with the lead isotope method in the Wangji-azhuang copper ore deposit of Zouping, Shandong province. *Geophys. Geochem. Explor.* **2014**, *38*, 23–27. (In Chinese with English Abstract)
108. Liu, X.M.; Chen, Y.L.; Wang, X.Q. Research on isotope identification for anomalous sources of deep-penetration geochemistry: Two cases of Jinwozi Au deposit, Xinjiang and Bairendaba-Weilasituo Polymetallic Deposit, Inner Mongolia. *Geoscience* **2012**, *26*, 1104–1116. (In Chinese with English Abstract)
109. Gao, Y.Y.; Wang, M.Q.; Yang, X.U. Study on the geogas composition of the concealed metal deposit and its background area: Take Zhangquanzhuang gold deposit as an example. *Geol. Surv. Res.* **2010**, *33*, 198–206. (In Chinese with English Abstract)
110. Wang, Y.; Ye, R.; Zhang, B.M.; Yang, R.; Qi, F.Y. The tentative geogas survey in the Jinwozi Concealed V210 gold deposit of Gobi area. *Geophys. Geochem. Explor.* **2012**, *36*, 263–266. (In Chinese with English Abstract)
111. Zhang, X.N.; Wang, M.Q.; Xu, G.M. Distortion reason of geogas to indicate concealed deposits and its reacting mechanism. *Geol. Surv. Res.* **2007**, *30*, 178–185. (In Chinese with English Abstract)
112. Lu, F.L. Pilot Study of Geogas Geochemical Exploration for Coverage Area in Arongqi, Inner Mongolia. Master Thesis, China University of Geosciences (Beijing), Beijing, China, 2019. (In Chinese with English Abstract).
113. Wang, X.J.; Lu, M.; Wang, Z.K.; Ye, R. Characteristics of geogas anomalies measured in the Shenjiayao gold deposit of Shan county, Henan province. *Geol. Explor.* **2016**, *52*, 667–677. (In Chinese with English Abstract)
114. Voltattorni, N.; Lombardi, S.; Beaubien, S.E. Gas migration from two mine districts: The Tolfa (Lazio, Central Italy) and the Neves-Corvo (Baixo Alentejo, Portugal) case studies. *J. Geochem. Explor.* **2015**, *152*, 37–53. [[CrossRef](#)]
115. Hu, X.Y.; Cao, J.J. Effect of quaternary sediments of Hengyang basin, Hunan on geo-gas prospecting. *Metal Mine* **2009**, *400*, 111–113. (In Chinese with English Abstract)
116. Hinkle, M.E. Environmental conditions affecting concentrations of He, CO₂, O₂ and N₂ in soil gases. *Appl. Geochem.* **1994**, *9*, 53–63. [[CrossRef](#)]
117. Mi, Y.B.; Cao, J.J.; Wu, Z.Q.; Wang, Z.H. Transmission electron microscopy analysis on fault gouges from the depths of the Bairendaba polymetallic deposit, Inner Mongolia, China. *J. Nanosci. Nanotechnol.* **2017**, *17*, 6549–6557. [[CrossRef](#)]
118. Hu, G.; Cao, J.J. Occurrence and significance of natural ore-related Ag nanoparticles in groundwater systems. *Chem. Geol.* **2019**, *515*, 9–21. [[CrossRef](#)]

119. Liu, X.; Cao, J.J.; Dang, W.Q.; Lin, Z.X.; Qiu, J.W. Nanoparticles in groundwater of the Qujia deposit, eastern China: Prospecting significance for deep-seated ore resources. *Ore Geol. Rev.* **2020**, *120*, 103417. [[CrossRef](#)]
120. Hu, G.; Cao, J.J.; Wang, C.Y.; Lu, M.Q.; Lin, Z.X. Study on the characteristics of naturally formed TiO₂ nanoparticles in various surficial media from China. *Chem. Geol.* **2020**, *550*, 119703. [[CrossRef](#)]
121. Yi, Z.B.; Cao, J.J.; Jiang, T.; Wang, Z.Y. Characterization of metal-bearing particles in groundwater from the Weilasituo Zn-Cu-Ag deposit, Inner Mongolia, China: Implications for mineral exploration. *Ore Geol. Rev.* **2020**, *117*, 103270. [[CrossRef](#)]
122. Ge, L.Q.; Tong, C.H.; Shen, S.P.; Yang, F.G.; Xiong, S.T. Geogas characters on concealed fault zone. *Nucl. Technol.* **1998**, *21*, 238–241. (In Chinese with English Abstract)
123. Mörner, N.A.; Etiope, G. Carbon degassing from the lithosphere. *Global Planet. Chang.* **2002**, *33*, 185–203. [[CrossRef](#)]
124. Cao, J.J.; Li, Y.K.; Jiang, T.; and Hu, G. Sulfur-containing particles emitted by concealed sulfide ore deposits: An unknown source of sulfur-containing particles in the atmosphere. *Atmos. Chem. Phys.* **2015**, *15*, 6959–6969. [[CrossRef](#)]
125. Lippmann-Pipke, J.; Erzinger, J.; Zimmer, M.; Kujawa, C.; Boettcher, M.; Van Heerden, E.; Bester, A.; Moller, H.; Stroncik, N.A.; Reches, Z. Geogas transport in fractured hard rock—Correlations with mining seismicity at 3.54 km depth, TauTona gold mine, South Africa. *Appl. Geochem.* **2011**, *26*, 2134–2146. [[CrossRef](#)]
126. Tong, C.H.; Li, X.L.; Li, J.C.; Wu, X.P. Geogas method—a new technique of searching for deep or concealed gold deposits. *Comput. Tech. Geophys. Geochem. Explor.* **1996**, *18*, 13–16. (In Chinese with English Abstract)
127. Cao, J.J. The effect factors and the present state of geogas measurement study. *Hunan Geol.* **2001**, *20*, 154–156. (In Chinese with English Abstract)
128. Zhu, J.; Zhou, S.C.; Liu, J.; Wang, X.H.; Zhang, G.Y. Discussion of factors affecting results of geogas prospecting. *Mod. Min.* **2014**, *537*, 62–64. (In Chinese)
129. Adushkin, V.V.; Andreev, S.N.; Popel, S.I. Cavitation mechanism of formation of nano- and microsize particles of minerals in ore deposits. *Geol. Ore Deposits.* **2004**, *46*, 313–320.
130. Filimonova, L.G.; Trubkin, N.V. Micro- and nanoparticles of zincite and native zinc from disseminated mineralization of metasedimentary rocks in the Dukat ore field. *Geol. Ore Deposits* **2008**, *50*, 135–144. [[CrossRef](#)]
131. Hough, R.M.; Noble, R.R.P.; Hitchen, G.J.; Hart, R.; Reddy, S.M.; Saunders, M.; Clode, P.; Vaughan, D.; Lowe, J.; Gray, D.J.; et al. Naturally occurring gold nanoparticles and nanoplates. *Geology* **2008**, *36*, 571–574. [[CrossRef](#)]
132. González-Jiménez, J.M.; Reich, M. An overview of the platinum-group element nanoparticles in mantle-hosted chromite deposits. *Ore Geol. Rev.* **2017**, *81*, 1236–1248. [[CrossRef](#)]
133. Verdugo-Ihl, M.R.; Ciobanu, C.L.; Slattery, A.; Cook, N.J.; Ehrig, K.; Courtney-Davies, L. Copper-arsenic nanoparticles in hematite: Fingerprinting fluid-mineral interaction. *Minerals* **2019**, *9*, 388. [[CrossRef](#)]
134. Li, R.H.; Wang, X.Q.; Yang, L.Q.; Zhang, B.M.; Liu, Q.Q.; Liu, D.S. The characteristic of microstructural deformation of gold bearing pyrite in Jiaodong: The links between nanoscale gold enrichment and crystal distortion. *Ore Geol. Rev.* **2020**, *122*, 103495. [[CrossRef](#)]
135. Adushkin, V.V.; Andreev, S.N.; Popel, S.I. Formation of nano- and microspherules of minerals in ore deposits depending on depth of host rock occurrence. *Geol. Ore Depos.* **2006**, *48*, 237–243. [[CrossRef](#)]
136. Wang, X.Q.; Zhang, B.M.; Liu, X.M. Nanogeochemistry: Deep-penetrating geochemical exploration through cover. *Earth Sci. Front.* **2012**, *19*, 101–112. (In Chinese with English Abstract)
137. Yi, Z.B.; Fu, W.; Zhao, Q.; Lu, H.T.; Fu, X.N.; Li, P.Q.; Luo, P.; Han, Z.X.; Tan, Z.Q.; Xu, C. Characterization of nano-minerals and nanoparticles in supergene rare earth element mineralization related to chemical weathering of granites. *Am. Mineral.* **2023**, *108*, 1461–1475. [[CrossRef](#)]
138. Ciobanu, C.L.; Cook, N.J.; Utsunomiya, S.; Kogagwa, M.; Green, L.; Gilbert, S.; Wade, B. Gold-telluride nanoparticles revealed in arsenic-free pyrite. *Am. Mineral.* **2012**, *97*, 1515–1518. [[CrossRef](#)]
139. Deditius, A.P.; Utsunomiya, S.; Reich, M.; Kesler, S.E.; Ewing, R.C.; Hough, R.; Walshe, J. Trace metal nanoparticles in pyrite. *Ore Geol. Rev.* **2011**, *42*, 32–46. [[CrossRef](#)]
140. Ye, R.; Zhang, B.M.; Wang, Y. Mechanism of the migration of gold in desert regolith cover over a concealed gold deposit. *Geochem. Explor. Environ. Anal.* **2015**, *15*, 62–71. [[CrossRef](#)]
141. Fairbrother, L.; Brugger, J.; Shapter, J.; Laird, J.S.; Southam, G.; and Reith, F. Supergene gold transformation: Biogenic secondary and nano-particulate gold from arid Australia. *Chem. Geol.* **2012**, *320*, 17–31. [[CrossRef](#)]
142. Zhmodik, S.M.; Kalinin, Y.A.; Roslyakov, N.A.; Mironov, A.G.; Mikhlin, Y.L.; Belyanin, D.K.; Nemirovskaya, N.A.; Spiridonov, A.M.; Nesterenko, G.V.; Airiyants, E.V.; et al. Nanoparticles of noble metals in the supergene zone. *Geol. Ore Deposits* **2012**, *54*, 141–154. [[CrossRef](#)]
143. Shuster, J.; Lengke, M.; Márquez-Zavalía, M.F.; Southam, G. Floating gold grains and nanophase particles produced from the biogeochemical weathering of a gold-bearing ore. *Econ. Geol.* **2016**, *111*, 1485–1494. [[CrossRef](#)]
144. Liu, R.; Cao, J.J.; Deng, Y.K.; Wang, G.Q.; Liu, X. Formation of nano- or near-nanoparticles via oxidation in the Dabaoshan concealed deposit, Guangdong province. *Arab. J. Geosci.* **2020**, *13*, 1061. [[CrossRef](#)]
145. Osovetsky, B.M. Aggregation of nanogold particles in the environment. *Nat. Resour. Res.* **2016**, *25*, 241–253. [[CrossRef](#)]
146. Reith, F.; Cornelis, G. Effect of soil properties on gold- and platinum nanoparticle mobility. *Chem. Geol.* **2017**, *466*, 446–453. [[CrossRef](#)]

147. Fu, Y.H.; Wan, Q.; Qin, Z.H.; Nie, X.; Yu, W.B.; Li, S.S. The effect of pH on the sorption of gold nanoparticles on illite. *Acta Geochim.* **2020**, *39*, 172–180. [[CrossRef](#)]
148. Christenson, B.W.; Malmqvist, L.; Kristiansson, K.; Finlayson, J.B. Soil Gas Trace Metal Transport-The GEOGAS Method Applied to NZ Epithermal and Geothermal Environments. In Proceedings of the 10th New Zealand Geothermal Workshop, Geothermal Institute of the University of Auckland and the Centre for Continuing Education, Auckland, New Zealand, 2–4 November 1988; pp. 155–160. [[CrossRef](#)]
149. He, D.F. Structure of unconformity and its control on hydrocarbon accumulation. *Petrol. Explor. Dev.* **2007**, *34*, 142–149. (In Chinese with English Abstract)
150. Zou, C.N.; and Tao, S.Z. Geological characteristics of large gas provinces and large gas fields in China. *Sci. China Ser. D* **2008**, *51*, 14–35. [[CrossRef](#)]
151. Plet, C.; Noble, R.R.P. Soil gases in mineral exploration: A review and the potential for future developments. *Geochem. Explor. Environ. Anal.* **2023**, *23*, geochem2023-008. [[CrossRef](#)]
152. Hu, G.; Cao, J.J.; Lai, P.X.; Hopke, P.K.; Holub, R.F.; Zeng, J.N.; Wang, Z.H.; Wu, Z.Q. Characteristics and geological significance of particles on fractures from the Dongshengmiao polymetallic pyrite deposit, Inner Mongolia, China. *Geochem. Explor. Environ. Anal.* **2015**, *15*, 373–381. [[CrossRef](#)]
153. Wang, G.Q.; Cao, J.J.; Dai, D.L. TEM analysis of nano-or near-nanoparticles in fault gouge from the Kaxiutata iron deposit (CHN) and the implications for ore body exploration. *J. Geochem. Explor.* **2019**, *207*, 106390. [[CrossRef](#)]
154. Lu, M.; Cao, J.J.; Wang, Z.Y.; Wang, G.Q. Characteristics of Naturally Formed Nanoparticles in Various Media and Their Prospecting Significance in Chaihulanzi Deposit. *Minerals* **2022**, *12*, 1289. [[CrossRef](#)]
155. Zhang, B.M.; Wang, X.Q.; Han, Z.X.; Liu, H.L.; Liu, D.S.; Lu, Y.X.; Sun, B.B. Evidence of metal migration over concealed gold deposit in loess terrain and its prospecting significance. *Appl. Geochem.* **2022**, *145*, 105422. [[CrossRef](#)]
156. Li, J.; Zhang, B.M.; Gong, Q.J.; Liu, H.L.; Liu, N.Q. Microscopic Morphology and Indicative Significance of Nanoscale Au Particles in Soils and Fault Muds: A Case Study of Jiaojia, Shandong Province. *Appl. Sci.* **2023**, *13*, 2126. [[CrossRef](#)]
157. Wang, X.Q.; Xu, S.F.; Chi, Q.H.; Liu, X.M. Gold geochemical provinces in China: A micro- and nanoscale formation mechanism. *Acta Geol. Sin.* **2013**, *87*, 1–8. (In Chinese with English Abstract)
158. Anand, R.R.; Aspandiar, M.F.; Noble, R.R.P. A review of metal transfer mechanisms through transported cover with emphasis on the vadose zone within the Australian regolith. *Ore Geol. Rev.* **2016**, *73*, 394–416. [[CrossRef](#)]
159. Reith, F.; Stewart, L.; Wakelin, S.A. Supergene gold transformation: Secondary and nano-particulate gold from southern New Zealand. *Chem. Geol.* **2012**, *320*, 32–45. [[CrossRef](#)]
160. Sanyal, S.K.; Shuster, J.; Reith, F. Cycling of biogenic elements drives biogeochemical gold cycling. *Earth-Sci. Rev.* **2019**, *190*, 131–147. [[CrossRef](#)]
161. Wang, D.H.; Liu, L.J.; Hou, J.L.; Dai, H.Z.; Tian, S.H. A preliminary review of the application of “five levels + basement” model for Jiajika-style rare metal deposits. *Earth Sci. Front.* **2017**, *24*, 1–7. (In Chinese with English Abstract)
162. Dai, H.Z.; Wang, D.H.; Liu, L.J.; Yu, Y.; Dai, J.J. Geochronology and geochemistry of Li (Be)-bearing granitic pegmatites from the Jiajika superlarge Li-polymetallic deposit in Western Sichuan, China. *J. Earth Sci. China* **2019**, *30*, 707–727. [[CrossRef](#)]
163. Xia, X.H. Ore-forming characteristics and genetic discussion of the Dongshengmiao polymetallic pyrite deposits in the Langshan Metallogenic Belt, Inner Mongolia. *Miner. Depos.* **1992**, *11*, 374–383. (In Chinese with English Abstract)
164. Guo, Z.J.; Kong, M.; Zhang, H.; Yang, F.; Xu, R.T.; Wang, C.W.; Wang, Q.B.; Song, Y.T.; Han, W. Landscape division suitable for geochemical exploration. *Geophys. Geochem. Explor.* **2015**, *39*, 12–15. (In Chinese with English Abstract)
165. Liu, D.S.; Chi, Q.H.; Wang, X.Q.; Chen, Y.Y.; Nie, L.S.; Yang, F. National-Scale Cobalt Geochemical Mapping of Exposed Crust in China. *Minerals* **2022**, *12*, 1220. [[CrossRef](#)]
166. Sun, Z.J.; Liu, Z.H.; Yu, Z.W.; Li, W.C.; Liang, J.Q. The disturbance mechanism of the eolian sand to the migration of ore-forming elements in stream sediments in Qinghai province. *Geophys. Geochem. Explor.* **2003**, *27*, 167–170. (In Chinese with English Abstract)
167. Yu, J.S.; Sun, Z.J.; Zhang, H.; Liu, H.Z.; Cen, K. Detail landscape soil survey technology for high-cold limnetic hills in the Qinghai province. *Geol. Prospect.* **2005**, *41*, 56–59. (In Chinese with English Abstract)
168. Wang, B.L.; French, H.M. Climate controls and high-altitude permafrost, Qinghai-Xizang (Tibet) Plateau, China. *Permafrost. Periglac. Process.* **1994**, *5*, 87–100. [[CrossRef](#)]
169. Wu, Q.B.; Zhang, T.J.; Liu, Y.Z. Permafrost temperatures and thickness on the Qinghai-Tibet Plateau. *Glob. Planet. Chang.* **2010**, *72*, 32–38. [[CrossRef](#)]

Disclaimer/Publisher’s Note: The statements, opinions and data contained in all publications are solely those of the individual author(s) and contributor(s) and not of MDPI and/or the editor(s). MDPI and/or the editor(s) disclaim responsibility for any injury to people or property resulting from any ideas, methods, instructions or products referred to in the content.